

# UC San Diego

## UC San Diego Electronic Theses and Dissertations

### Title

Effect of small linear motion on the accuracy of estimating coronary vessel stenosis in Cardiac Computed Tomography

### Permalink

<https://escholarship.org/uc/item/4v15k72j>

### Author

Budhiraja, Suhas

### Publication Date

2017

### Supplemental Material

<https://escholarship.org/uc/item/4v15k72j#supplemental>

Peer reviewed|Thesis/dissertation

UNIVERSITY OF CALIFORNIA, SAN DIEGO

Effect of small linear motion on the accuracy of estimating coronary vessel stenosis in  
Cardiac Computed Tomography

A Thesis submitted in partial satisfaction of the requirements  
for the degree Master of Science

in

Bioengineering

by

Suhas Budhiraja

Committee in charge:

Professor Elliot R. McVeigh, Chair

Professor Todd P. Coleman

Professor Thomas T. Liu

2017

©

Suhas Budhiraja, 2017

All rights reserved

The Thesis of Suhas Budhiraja is approved, and it is acceptable in quality and form for publication on microfilm and electronically.

---

---

---

Chair

University of California, San Diego

2017

## **DEDICATION**

**This work would have never been possible without**

**My Father, whom I can't thank enough for being the most inspirational life story**

**My Mother, who always says that I can**

**My Guru, Elliot McVeigh, who guided me through this**

**And of course, the Almighty for being by my side.**

## **EPIGRAPH**

**Perception is the true reality.**

**Change your perception; change your reality.**

# TABLE OF CONTENTS

|  |             |
|--|-------------|
| <b>Signature Page</b> .....  | <b>iii</b>  |
| <b>Dedication</b> .....  | <b>iv</b>   |
| <b>Epigraph</b> .....  | <b>v</b>    |
| <b>Table of Contents</b> .....   | <b>vi</b>   |
| <b>List of Abbreviations</b> .....   | <b>viii</b> |
| <b>List of Figures</b> .....   | <b>ix</b>   |
| <b>List of Supplemental Files</b> .....  | <b>xii</b>  |
| <b>Acknowledgements</b> .....  | <b>xiii</b> |
| <b>Abstract of the Thesis</b> .....  | <b>xv</b>   |
| <b>Chapter 1: Background</b> .....   | <b>1</b>    |
| <b>1.1 Introduction</b> .....  | <b>1</b>    |
| <b>1.2 Computed Tomography</b> .....   | <b>3</b>    |
| <b>1.2.1 CT Metrics</b> .....  | <b>4</b>    |
| <b>1.3 Coronary Geometry</b> .....   | <b>7</b>    |
| <b>1.4 Patient Protocol</b> .....  | <b>7</b>    |
| <b>1.5 Effectiveness of CT Procedures</b> .....  | <b>8</b>    |
| <br>   |             |
| <b>Chapter 2: Methods to evaluate degree of stenosis</b> .....                                 | <b>10</b>   |
| <b>2.1 Common Methods</b> .....  | <b>10</b>   |
| <b>2.2 Fractional Flow Reserve</b> .....   | <b>10</b>   |
| <b>2.3 CT Resolution and factors affecting CT Resolution</b> .....                             | <b>12</b>   |
| <br>   |             |
| <b>Chapter 3: Literature Survey</b> .....  | <b>14</b>   |
| <br>   |             |
| <b>Chapter 4: Coronary motion characterization with high resolution X-Ray angiography</b> .... | <b>17</b>   |
| <b>4.1 Introduction</b> .....  | <b>17</b>   |
| <b>4.2 Purpose</b> .....   | <b>17</b>   |
| <b>4.3 Methods</b> .....   | <b>18</b>   |
| <b>4.4 Results</b> .....   | <b>20</b>   |
| <b>4.5 Conclusion and Discussion</b> .....   | <b>27</b>   |

|   |           |
|---|-----------|
| <b>Chapter 5: Signal intensity characterization with geometry and orientation .....</b> | <b>29</b> |
| <b>5.1 Introduction.....</b>  | <b>29</b> |
| <b>5.2 Purpose.....</b>   | <b>30</b> |
| <b>5.3 Methods.....</b>   | <b>30</b> |
| <b>5.4 Results.....</b>   | <b>36</b> |
| <b>5.5 Conclusion and Discussion .....</b>  | <b>41</b> |
| <br>  |           |
| <b>Chapter 6: Signal intensity characterization with cardiac motion.....</b>            | <b>43</b> |
| <b>6.1 Introduction.....</b>  | <b>43</b> |
| <b>6.2 Purpose.....</b>   | <b>43</b> |
| <b>6.3 Methods.....</b>   | <b>44</b> |
| <b>6.4 Results.....</b>   | <b>46</b> |
| <b>6.5 Conclusion and Discussion .....</b>  | <b>49</b> |
| <br>  |           |
| <b>Chapter 7: Limitations .....</b>   | <b>50</b> |
| <br>  |           |
| <b>Chapter 8: Future work .....</b>   | <b>51</b> |
| <br>  |           |
| <b>References.....</b>  | <b>52</b> |

## LIST OF ABBREVIATIONS

|             |  |
|-------------|--|
| CAD.....    | Coronary Artery Disease                      |
| CT.....     | Computed Tomography                          |
| CCTA.....   | Coronary Computed Tomography Angiography     |
| IHD.....    | Ischemic Heart Diseases                      |
| MI.....     | Myocardial Infarction                        |
| HF.....     | Heart Failure                                |
| CTA.....    | Computed Tomography Angiography              |
| MTF.....    | Modulation Transfer Function                 |
| ECG.....    | Electro Cardio Graph                         |
| NPV.....    | Negative Predictive Value                    |
| FFR.....    | Fractional Flow Reserve                      |
| FFR-CT..... | Fractional Flow Reserve- Computed Tomography |
| EM.....     | Electro Magnetic                             |
| IVUS.....   | IntraVascular Ultrasound                     |
| Ao.....     | Aorta  |
| LM.....     | Left Main Artery                             |
| LAD.....    | Left Anterior Descending Artery              |
| LCX.....    | Left Circumflex Artery                       |
| RCA.....    | Right Coronary Artery                        |
| HU.....     | Hounsfield Units                             |
| FWHM.....   | Full Width Half Maximum                      |
| NIH.....    | National Institutes of Health                |
| ROI.....    | Region of Interest                           |
| AHA.....    | American Heart Association                   |

## LIST OF FIGURES

|                   |  |    |
|-------------------|--|----|
| <b>Figure 1.1</b> | Labelled heart diagram .....   | 1  |
| <b>Figure 1.2</b> | The inside view of normal v/s atherosclerotic artery .....   | 3  |
| <b>Figure 1.3</b> | GE VCT scanner 64 slice.....   | 4  |
| <b>Figure 1.4</b> | View of coronary artery and ventricles with injected contrast, made using high-resolution scanner .....  | 6  |
| <b>Figure 1.5</b> | Coronary segments and their position over myocardium .....   | 7  |
| <b>Figure 2.1</b> | Description of FFR procedure .....   | 11 |
| <b>Figure 2.2</b> | Inside-vessel view catheter to measure FFR.....  | 12 |
| <b>Figure 3.1</b> | Angiographically non-obstructive lesion of the left anterior descending artery..   | 15 |
| <b>Figure 4.1</b> | Labelled coronary segments per AHA.....  | 19 |
| <b>Figure 4.2</b> | Velocity profile of various coronary segments along the R-R frames.....  | 20 |
| <b>Figure 4.3</b> | (a) Relative position of coronary tree at a certain frame in R-R interval with respect to frame 1 of R-R interval (end diastole) (b) Color coded velocity value at a certain frame in R-R interval ..... | 21 |
| <b>Figure 4.4</b> | Velocity profile of various coronary segments for Case003(1) along the R-R frames .....  | 22 |
| <b>Figure 4.5</b> | Velocity profile of various coronary segments for Case003(3) along the R-R frames .....  | 22 |
| <b>Figure 4.6</b> | Velocity profile of various coronary segments for Case002(3) along the R-R frames .....  | 23 |
| <b>Figure 4.7</b> | Velocity profile of various coronary segments for Case004(2) along the R-R frames .....  | 23 |
| <b>Figure 4.8</b> | Velocity profile of various coronary segments for Case001b(2) along the R-R frames .....   | 24 |
| <b>Figure 4.9</b> | Velocity profile of various coronary segments for Case001b(6) along the R-R frames .....   | 24 |

|                    |  |    |
|--------------------|--|----|
| <b>Figure 4.10</b> | Velocity profile of LCX distal segment along the R-R segments in various subjects .....  | 25 |
| <b>Figure 4.11</b> | Velocity profile of LCX proximal segment along the R-R segments in various subjects .....  | 25 |
| <b>Figure 4.12</b> | Velocity profile of LAD proximal segment along the R-R segments in various subjects .....  | 26 |
| <b>Figure 4.13</b> | Velocity profile of RCA distal segment along the R-R segments in various subjects .....  | 26 |
| <b>Figure 4.14</b> | Distribution showing number of segments having various amounts of motion...  | 27 |
| <b>Figure 4.15</b> | Distribution showing number of segments in various duration of diastasis .....   | 28 |
| <b>Figure 5.1</b>  | CT image of physical phantom with holes of different diameter sizes (in mm), marked .....  | 31 |
| <b>Figure 5.2</b>  | Cropped view of diameter hole size 3.5 mm, as observed in the CT scan .....  | 31 |
| <b>Figure 5.3</b>  | Relative intensity with respect to diameter per digital simulation [46] .....  | 32 |
| <b>Figure 5.4</b>  | Coronary tree generated by Medis QAngio with labelled segments .....   | 33 |
| <b>Figure 5.5</b>  | (a) Longitudinal view of a coronary vessel in Medis QAngio (b) Transverse view of one slice in the corresponding vessel in (a) ..... | 34 |
| <b>Figure 5.6</b>  | Relative intensity with respect to observed diameter in LAD of a human heart .   | 35 |
| <b>Figure 5.7</b>  | Relative intensity with respect to diameter values in phantom.....   | 36 |
| <b>Figure 5.8</b>  | Relative intensity with respect to observed diameter in LAD of Patient 000.....  | 37 |
| <b>Figure 5.9</b>  | Relative intensity with respect to observed diameter in LCX of Patient 000.....  | 37 |
| <b>Figure 5.10</b> | Relative intensity with respect to observed diameter in LCX of Patient 005.....  | 38 |
| <b>Figure 5.11</b> | Relative intensity with respect to observed diameter in LCX of Patient 020 (75% of R-R).....   | 38 |
| <b>Figure 5.12</b> | Relative intensity with respect to observed diameter in LCX of Patient 020 (80% of R-R).....   | 39 |
| <b>Figure 5.13</b> | Relative intensity with respect to observed diameter in LCX of Patient 023.....  | 39 |
| <b>Figure 5.14</b> | Relative intensity with respect to observed diameter in RCA of Patient 023.....  | 40 |

|                    |   |    |
|--------------------|---|----|
| <b>Figure 5.15</b> | Relative intensity with respect to observed diameter in LCX of Patient 026 .....  | 40 |
| <b>Figure 5.16</b> | Relative intensity with respect to observed diameter for entire patient dataset (average trend in black) .....                        | 41 |
| <b>Figure 6.1</b>  | NRT 100 motor from Thorlabs .....   | 44 |
| <b>Figure 6.2</b>  | Set up of phantom and motor assembly to scan for studying motion effects on CT image.....   | 45 |
| <b>Figure 6.3</b>  | Plot showing the trend of intensity values with real diameter values .....  | 47 |
| <b>Figure 6.4</b>  | Plot showing the trend of intensity values using digital phantom [46].....  | 47 |
| <b>Figure 6.5</b>  | Plot showing the trend of intensity values in LAD of Patient 000 at 75%, 80% and 85 <sup>th</sup> time frame during R-R interval..... | 48 |
| <b>Figure 6.6</b>  | Plot showing the trend of intensity values in LCX of Patient 020 at 75% and 80 <sup>th</sup> time frame during R-R interval .....     | 49 |

## LIST OF SUPPLEMENTAL FILES

### 1. **chapter\_4\_movies.zip**

- 1.1 Case\_001b\_2.avi
- 1.2 Case\_001b\_6.avi
- 1.3 Case\_002\_3.avi
- 1.4 Case\_003\_1.avi
- 1.5 Case\_003\_3.avi
- 1.6 Case\_004\_2.avi

### 2. **analysis\_data.zip**

- 2.1 Patient\_000\_LAD\_Analysis\_phase\_75
- 2.2 Patient\_000\_LAD\_Analysis\_phase\_75
- 2.3 Patient\_000\_LAD\_Analysis\_phase\_75
- 2.4 Patient\_000\_LAD\_Analysis\_phase\_75
- 2.5 Patient\_000\_LAD\_Analysis\_phase\_75
- 2.6 Patient\_000\_LAD\_Analysis\_phase\_75
- 2.7 Patient\_000\_LAD\_Analysis\_phase\_75
- 2.8 Patient\_000\_LAD\_Analysis\_phase\_75
- 2.9 Patient\_000\_LAD\_Analysis\_phase\_75
- 2.10 Patient\_000\_LAD\_Analysis\_phase\_75

### 3. **phantom\_specs.pdf**

## ACKNOWLEDGEMENTS

To my mentor, Dr. Elliot McVeigh. Thank you for giving me this opportunity to work with you and making my dream of working in medical world come true. Thank you for being so kind, supportive and ever so encouraging.

I would like to express my sincere gratitude for Dr. Francisco Contijoch for his valuable and continuous support during my entire tenure at McVeigh lab. I couldn't have done this without him.

I would also like to thank Andrew Schluchter, our lab manager for being a wonderful person and offering a helping hand every time I needed. I would also like to thank him for our discussions about science and life. I am also thankful to the lab members of the Cardiovascular Imaging Lab (CViL); Zhenngong Chen, Ali Ashitani, Teo Dinescu, and all the others for being a part of this journey and helping in their own individual ways.

I would like to thank my committee members, Dr. Todd P. Coleman and Dr. Thomas T. Liu, for their time, consideration and motivation.

To my parents, without whom I would haven't been able to come this far in my life. I would also like to thank my brother, Bhavye for being there when it mattered.

I would also like to thank my friends at UCSD, Shravani and Padmaja, for their constant support in making me through my years in San Diego.

I would also like to thank my friends Ridhima, Surabhi, Aditya, Navraj, Karan, Vishesh, and Sargam for their constant motivation and emotional support in their unique ways.

I would like to end by thanking the Department of Bioengineering at University of California San Diego for giving me the wonderful platform and the department coordinators for their constant help and smooth administration.

## **ABSTRACT OF THE THESIS**

Effect of small linear motion on the accuracy of estimating coronary vessel stenosis in  
Cardiac Computed Tomography

by

Suhas Budhiraja

Master of Science in Bioengineering

University of California, San Diego, 2017

Professor Elliot R. McVeigh, Chair

Coronary Artery Diseases (CAD) are believed to be the most common form of heart diseases and the leading cause of deaths of both men and women in the United States. The diagnosis of CAD is largely dependent on various medical imaging procedures and the experience of the radiologists and cardiologists to form a diagnosis based upon those

images. In case of using Coronary Computed Tomography Angiography (CCTA) to assess coronary vessel stenosis, the geometry of the vessels and the cardiac rhythm can alter the image produced during the scan.

There is a need to study the effects of these artifacts on the image, as it could largely impact the decision of calling a vessel stenosis. These artifacts cause an increasing number of false positive diagnosis, thereby leading several patients without lesions or stenosis to catheterization. The small motion causes changes in the signal intensity in those lesions, leading to incorrect diagnosis. Hence, based on the results of the previous computer simulation research done on the effects of coronary geometry and motion on the CT images, a similar study is aimed on the physical phantom and some real patient data set. We aim to characterize motion in the coronary arteries and make inferences about suggestive CT procedures or post processing required after a CCTA. A part of this study involved doing real time CT scans on phantom and using pre-recorded CT data. The outcome of the research is the various trends in motion and the effect of that motion on the intensity of the resulting images.

# CHAPTER 1: BACKGROUND

## 1.1 Introduction

I would like to start this thesis by looking at this picture

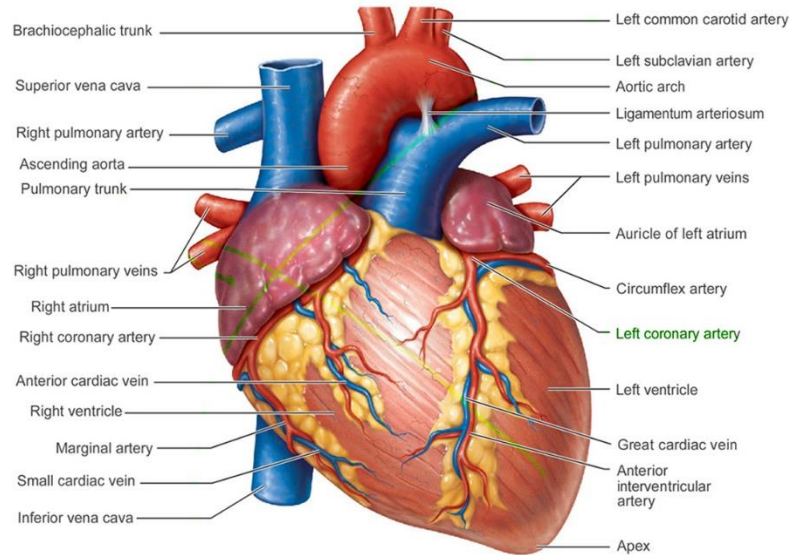


**Figure 1.1 Labelled heart diagram**

This is the first picture I looked at when I started my work in Cardiovascular domain. The cardiovascular system is complex. The complexity has been put up in literature and is dependent on several regulation mechanisms and cardiovascular variables [1]. There have been many publications in this field with different speculations about the pumping function of heart. Even after years of dedicated research, there hasn't been a complete understanding of this paramount body organ which works without any rest for the entire lifetime [2]. Cardiovascular diseases being one of the leading causes of deaths worldwide, accounting for almost a third of all the deaths [3], require quantitative and accurate measures for their early detection. In developed countries, ischemic heart disease and cerebrovascular disease are together responsible for 36% of all deaths [4]. In fact, the

mortality rates due to cardiovascular diseases are still increasing in the developing countries because of population, and global lifestyle changes [5]. There have been several breakthroughs in cardiovascular medicine but ischemic heart diseases (IHD), such as myocardial infarction (MI) and heart failure (HF) remain among the most important health challenges worldwide [6]. MI, due to coronary artery disease (CAD), is currently one of the major contributors to the development of HF [7]. CAD was found to be the reason for heart failure in 68% of the cases in a multicenter heart failure trial among over 20,000 patients [8].

Coronary artery disease (CAD) is the term for atherosclerosis in the coronary arteries. Atherosclerotic disease is the development of artery wall thickening and calcification, due to accumulation of lipids within the arterial intima resulting in atherosclerotic plaques. Atherosclerosis causes an increased peripheral resistance in the vasculature leading to increased burden on myocardium and in some cases, the extreme narrowing of blood vessels due to plaque building causes obstruction to blood flow, called stenosis. Due to this imbalance between the supply and demand, lack of oxygen occurs and leads to myocardial ischemia. Prolonged ischemia can lead to myocardial infarction, i.e. regional myocardial cell death/necrosis, more commonly known as heart attack. The most general cause of heart attack is CAD. Stable CAD is associated with chronic stenosis in the coronary arteries, causing symptoms such as angina (chest pain) at a particular work-load. In fact, stable CAD commonly causes constant or slowly progressive symptoms over time. A sudden change of symptoms is associated with unstable CAD, often due to a plaque rupture leading to thrombus formation in the artery. When a plaque ruptures and sub-endothelial vessel structures come into contact with the blood, a thrombus formation is

triggered, creating a dynamic stenosis or occlusion in the coronary artery. Unstable CAD have an even greater cardiac death risk and need medical attention right away.



**Figure 1.2 The inside view of a normal v/s atherosclerotic artery**

Hence, we have an idea as to how coronary stenosis can be dangerous in terms of cardiovascular health and needs to be treated right away. The treatment of any medical condition depends on the correct and suitable diagnostic technique. I am going to discuss about Computed Tomography and how it can serve as our diagnostic tool for safe and efficient diagnosis of a coronary stenosis and hence a CAD.

## **1.2 Computed Tomography**

A Computed Tomography (CT) scan is produced by a rotating x-ray tube emitting a fan-shaped x-ray beam usually through a patient, who is situated along the axis of rotation, and onto a row of detectors. The contrast mechanism is similar to that of X-ray angiography, although it is injected intravenously for a Coronary CT Angiography. CT requires numerous projection images at incremental angles which later reconstruct into a single volumetric dataset. The spatial resolution of CT is dependent on the electronics of the detector and the detector row spacing. This measure is approximately 0.5 mm in-plane,

and 0.5 - 0.625 mm through-plane [9,10]. For a 180° plus fan scan, the temporal resolution of CT depends on the time it takes for the gantry to rotate 180° plus the fan beam angle, which is the angular coverage required for partial data reconstruction. Minimum gantry rotation times are currently at approximately 270 ms, yielding a maximum temporal resolution of roughly 150 ms. To minimize cardiac motion artifacts, data is acquired during diastasis periods over multiple heartbeats and is retrospectively binned to form one sufficient dataset for reconstruction. Patients have to hold their breaths during the scanning procedure. At regular heart rates of 60 to 70 bpm, a 16-slice CT scanner will require a scan time of roughly 20 s, whereas a 64-slice scanner will require roughly 5 s.



**Figure 1.3 GE VCT scanner 64 slice**

### **1.2.1 CT Metrics**

The three major CT image quality metrics are spatial resolution, temporal resolution, and volume coverage. These are important as they impart the ability to resolve the difference between various tissues. The administration method of contrast media also effects the CTA acquisition. Spatial resolution measures the smallest high contrast object

depicted by the CT system and depends largely on the detector collimation and reconstruction kernel. The size of focal spot is yet another key parameter. Spatial resolution can be described in terms of the Modulation Transfer Function (MTF) of the system. Consider a set of equally spaced lines where the spaces have the same thickness as the lines. A “line pair” is defined as one line plus one space. The “spatial frequency” is measured in line pairs per centimeter. For instance, 5 line pairs per centimeter would refer to lines and spaces each 1 millimeter thick, the total of the 5 line pairs and spaces would occupy exactly one centimeter. The MTF describes how well the CT scanner can differentiate between the objects with different spatial frequencies. Larger objects with poorly defined edges have predominantly low spatial frequencies where as small objects with sharp edges have higher spatial frequencies. The spatial frequency of the smallest, sharpest object that the scanner can measure or image is its spatial resolution. CTA can generally assess arteries as small as 1 mm in diameter. Since CTA is volumetric, it gives a three-dimensional visual of the vascular system and the overlapping structures are easily separable. A CT scan can be used to image complex miniature coronary arteries as well as renal and neurovascular structure along with a complete examination of aorta. CT scan can image small, tortuous coronary arteries as well as the renal and neurovascular circulation, up to and including a comprehensive evaluation of the aorta [11].

Particularly for cardiac imaging, another important metric for CTA is temporal resolution. For cardiac imaging, superior temporal resolution is achieved from faster gantry rotation, dual source CT, and multi-segment reconstruction. Modern scanners have a gantry rotation time of 280-350 milliseconds. Hence, a volume element of data (3-4 cm on 64-detector row scanners) can be acquired with full scan mode in less than a half second.

However, for cardiac imaging, faster imaging is needed to decrease motion artifacts associated with the beating heart.



**Figure 1.4 View of coronary artery and ventricles with injected contrast, made using a high-resolution scanner**

The half-scan technique [12] uses data from a little over 50% of a gantry rotation to improve temporal resolution to 175 milliseconds or less. Dual source CT provides the best temporal resolution available by using two radiation sources to simultaneously acquiring different data projections [13]. This improves temporal resolution by a factor of two [14]; in coronary imaging, image quality is improved with a temporal resolution of 82.5 ms for higher heart rates [15-17]. Multi-segment reconstruction [18] uses less data per cardiac cycle at each z-axis location but acquires the additional projection data at the same z-axis location for a full half scan reconstruction from additional heartbeats. In practice, different sections of the image are obtained from different heartbeats. Multi-segment reconstruction increases patient radiation dose compared to single-segment reconstruction and is thus, prone to artifacts from beat to beat variation [19,20].

### 1.3 Coronary Geometry

Given below are the coronary artery segments according to the American Heart Association.

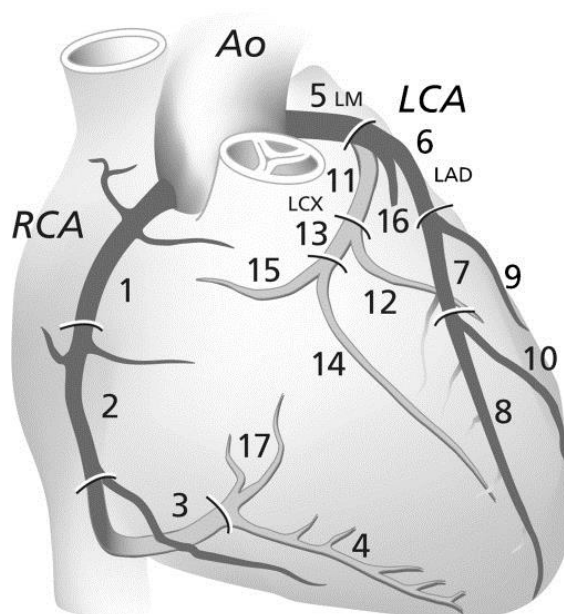


**Figure 1.5 Coronary segments and their position over myocardium**

### 1.4 Patient Protocol

A general Coronary Computed Tomography Angiography (CCTA) involves some preparation as follows:

The patient is asked to wear loose fitting clothes and is asked to remove any form of metal from his body, as much as possible. The patient is asked to fast beforehand for few hours since an iodine contrast agent is used. Beta-blocker medication may be given a night before to lower the heart rate in order to optimize the exam.

After the patient is ready to get scanned, he is asked to lie down on the scanner table. Two electrodes are stuck to the chest and connected to the ECG monitor, which

shows the heart's activity along the scan. A needle is inserted in a vein in the arm to inject the contrast material (iodine). Beta-blocker may be administered intravenously to slow down the heart if needed. Nitroglycerine is given as a tablet or as a spray under the tongue, to dilate the coronary arteries and hence improve their visualization. The patient is asked to hold his breath for 5-15 seconds. The table then moves through the scanner depending upon the type of scan and the data is thus acquired, for different time points along the heartbeat [21].

### **1.5 Effectiveness of CT Procedures**

There is ample data that establishes the detection accuracy of the presence and severity of coronary atherosclerosis using CCTA. There have been a large number of studies that compare CCTA with invasive angiography involving research on about 2000 patients [22,23]. In a 16-slice scanner based study that characterized 50% lesion as positive, resulted in an average sensitivity and specificity of 96% and 76% respectively (11 reports in 885 subjects) [22,24]. A comparable analysis for 64-slice scanners (7 studies in 444 subjects) confirms greater accuracy, with reported sensitivity and specificity of 98% and 93%, respectively [25,26]. A combined statistics for 18 studies, involving 1,329 subjects, the subject weighted mean sensitivity and specificity was 97% and 84%. There are few limitations due to a selective group of patients (those previously scheduled for invasive angiography) being chosen for the study, thus creating a bias towards patients likely to harbor disease, as reflected in the high incidence of true disease (mean 53%) in study subjects. According to the Bayes theorem, this bias might tend to increase the measured sensitivity and decrease the measured negative predictive value of CCTA. However, it is

impressive that even with this bias, the average subject-weighted negative predictive value(NPV) in these 18 studies is 97%. These data lead to the hypothesis that a normal CCTA may obviate the need for invasive angiography in properly selected clinical circumstances. The comparative capability of CCTA for quantitative analysis of coronary lesion severity has also been studied [27,28,29]. High correlation was found with invasive angiography (average Pearson correlation,  $r=0.72$ ), but with considerable standard deviation, which presently limits its quantitative accuracy. Hence, CCTA has a considerable high sensitivity and NPV for the detection of CAD [30].

## **CHAPTER 2: METHODS TO EVALUATE DEGREE OF STENOSIS**

### **2.1 Common Methods**

The most common method of classifying lesions on a CCTA is by comparing the size of lesion vessel with the size of normal vessel, just proximal or distal to the lesion. The most utilized approach is to classify the severity of stenosis as mild (0-50%), moderate (50-70%), or severe (>70%), based on visual interpretation [31,32]. Defining an absolute quantity for lesion diameter is challenging because the severe lesions mostly fall below a 1.5 mm dimension, which is close to the scanner resolution. In addition to dimensional limitations, vessels that never come to rest during the heart cycle also present a quantification challenge. In fact, the average velocity of the proximal coronary vessels during diastasis is about 10 mm/s [33,34] which means the vessels can move about 2.5 mm during a 250 ms gantry rotation.

Experienced and skilled interpreters can usually estimate coronary lesions using visual observation, but an objective quantitative approach would be a better way to classify the lesions. Quantitative techniques such as FFR-CT [35,36] or plaque characterization [37] require quantitative estimates of lesion geometry. This greatly increases the importance of accurate quantification because the prime source of uncertainty in the FFR-CT estimates arise due to uncertainty in the vessel geometry.

### **2.2 Fractional Flow Reserve**

Fractional flow reserve (FFR) is a technique used in coronary catheterization to measure pressure differences across a coronary artery stenosis (narrowing, usually due to

atherosclerosis) to determine the likelihood that the stenosis impedes oxygen delivery to the heart muscle (myocardial ischemia). During coronary catheterization, a catheter is inserted into the femoral (groin) or radial arteries (wrist) using a sheath and guidewire.

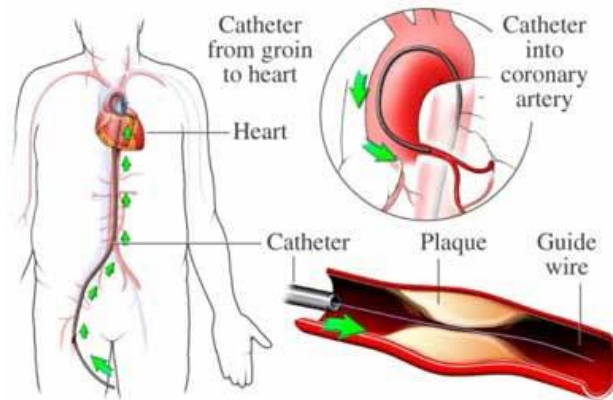


**Figure 2.1 Description of FFR procedure**

FFR uses a small sensor on the tip of the wire (commonly a transducer) to measure pressure, temperature and flow to determine the exact severity of the lesion. This is done during maximal blood flow (hyperemia), which can be induced by injecting products such as adenosine or papaverine. Fractional flow reserve (FFR) is the ratio of maximum blood flow distal to a stenotic lesion to normal maximum flow in the same vessel. It is calculated using the pressure ratio:

$$FFR = P_d/P_a$$

where  $P_d$  is the pressure distal to the lesion, and  $P_a$  is the pressure proximal to the lesion.



**Figure 2.2 Inside-vessel view with catheter to measure FFR**

FFR-CT is a technique to get FFR numbers using CT instead of invasive catheterization.

### **2.3 CT Resolution and factors affecting CT Resolution**

While performing a CT procedure on any tissue of the body, the resolution plays an important role. In case of buying a new phone, if you look for camera specifications, you keep in mind, the resolution of the camera. Same is the case with a CT scanner, because it's technically a camera or a device that clicks pictures of the insides of the body using electromagnetic field as its prime energy source (X-ray band of EM spectrum in contrast to the visible spectrum in case of a camera). On similar grounds, there are technical specifications that affect the quality of images produced using CT.

There are few elements of the CT scanner that effect the image resolution, like spot size, detector size, signal to noise ratio.

The key concept that this thesis talks about is the effect of motion on the resultant CT image thus produced.

During CT acquisition, the beating of the heart causes artifacts in the image produced. Imagine clicking a picture of a body in motion (for instance, a running man). If

you have a primitive camera with no motion correction, the resultant clicked image is nothing but a blurred reflection of the object under consideration.

The point further to be considered is that when we click a picture of a running man, we are aware about how the stationary man looks like and also, we know that the man was running in a particular direction. This knowledge enables us to comment on the quality of the image and we can say that it is blurred.

The above case is in complete contrast with the case of using CT to gather images of coronary arteries, which we know are moving since the heart is beating. The information that is missing is that we don't know how the coronary arteries actually look like, otherwise there wouldn't have been a need to image them using CT. Hence, there is no direct way of just looking at a CT image with coronary arteries in it and commenting on their realistic dimensions.

The following thesis talks about how motion can alter the appearance of the coronary arteries upon which the diagnosis greatly depends.

### **CHAPTER 3: LITERATURE SURVEY**

There has been much published work that documents the effect of motion artifacts, there is also research and documentation that made the motion measurements and suggested that motion affect the CCTA images. A study measured the cardiac and respiratory motion in various coronary arteries of the heart, using a 3D motion tracking algorithm [33].

However, before reaching to the effects of motion on CT procedures, more groundwork was done to understand the ability of CT techniques in the coronary vasculature world. The study of effectiveness of CCTA in detecting atherosclerotic plaques was done [38,39], paving a way for CCTA to be used as a method to find lesions in coronary arteries. The CCTA techniques were compared with other gold standard techniques used in evaluation of coronary lesions, such as Invasive Angiography and Intravascular Ultrasound [40]. This study aimed at finding diagnostic accuracy of CCTA when compared to invasive angiography and IVUS. The overall correlation in estimation of degree of stenosis using CT when compared to invasive angiography was found out to be  $r=0.54$ . The sensitivity of finding stenosis  $< 50\%$ , stenosis  $> 50\%$ , and stenosis  $> 75\%$  was found to be 79%, 73%, and 80%, respectively and specificity was found to be 97%. Compared to IVUS, 84% lesions were correctly identified with CT [40].

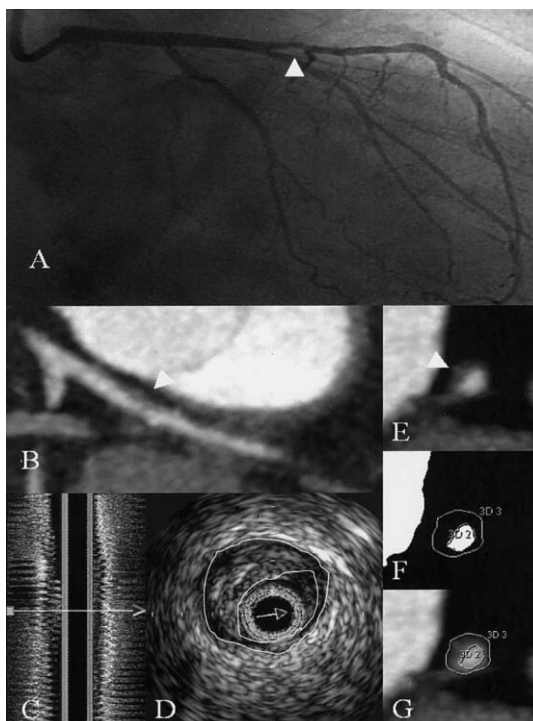


**Figure 3.1** Angiographically non-obstructive lesion of the left anterior descending artery. (A) Invasive angiogram: arrow indicates a non-obstructive smooth lesion. (B) 64-slice computed tomography: arrowheads indicate a noncalcified plaque in the left anterior descending artery. (C) Intravascular ultrasound: longitudinal reconstruction. (D) Intravascular ultrasound cross section: lumen area 4 mm<sup>2</sup>, plaque area 11 mm<sup>2</sup>. (E) Cross-sectional view of the coronary vessel. (F) Window setting for lumen measurements: width is reduced to 1 HU, window level is set to 65% (210 HU in this case) of the mean intensity measured in the lumen. (G) Window level to determine outer vessel boundaries (width at 155% of mean value within the lumen, level at 65% of mean value). Lumen area is 4 mm<sup>2</sup>, plaque area is 1 mm<sup>2</sup>. [40]

Efforts were made in order to estimate stenosis in coronary arteries using CCTA in the best way possible. A study was done in 2012 that used area based measurement in a physical phantom of coronary artery to quantify the stenosis in the arteries [41]. The mean measured degree of stenosis for a phantom with a 3-mm outer diameter was 49.0% ± 10.0% for 43.8% stenosis, 71.7% ± 9.6% for 75.0% stenosis, and 85.4% ± 5.9% for 93.8% stenosis. Algorithms are being developed to automatically detect various types of plaques and characterize them based on their severity and type [42].

All these studies involving CCTA to find coronary stenosis had some limitations involved with them. [41,42] The most commonly addressed issue was with the increased

X-ray radiation dose to the patients for prolonged scan duration required to get results in CCTA. Studies were done to estimate the dose of radiation that the patient was exposed to in an average CT scan [43]. This study suggested that an average CCTA uses 12 mSv dose of X-rays, which is 1.2 times the dose used in an abdominal CT or a dose equivalent to 600 chest X-rays. Various studies were done to estimate the 'safe' levels of radiation dose, and to compare the dose used in various procedures [44]. According to Occupational Safety and Health Administration at the US Department of Labor, the maximum permissible prospective annual dose limit is reported as 5 rems which is an equivalent of 50 mSv. Hence, the dosage used in CCTA lies within those limits.

Another major concern was the effect of cardiac motion on the quality of CT images. The motion of the heart degrades the image quality produced through CCTA [45]. A computer simulation study was done by Dr. Francisco Contijoch at University of California San Diego to estimate the effect of various vessel sizes and cardiac motion on the intensity of CT images, which led to the motivation of this thesis [46]. The study involved exploring the effect of small motions during CCTA acquisition on the vessel intensity and shape.

My work in association with this simulation study done at Cardiovascular Imaging Lab (CViL) at University of California San Diego involved creating a relationship between the image intensity in CCTA images and the varied degrees of motion and different vessel sizes.

## **CHAPTER 4: CORONARY MOTION CHARACTERIZATION WITH HIGH RESOLUTION XRAY ANGIOGRAPHY**

### **4.1 Introduction**

By far, we have established that there is in fact motion, because of the cardiac rhythm and that motion affects the resultant CT image produced during CCTA. The next step in this discussion would be to characterize the motion. There is a need to classify the varied degrees of motion that occur during the entire cycle of scan.

### **4.2 Purpose**

When a CCTA image is presented in front of a Cardiologist, a lot of things depend on the experience of the personnel apart from the visual appearance of the image. The effect of motion, left uncorrected can often lead to incorrect diagnosis and sending a person to invasive procedures without having the need to do so.

Thus, since we have enough background to confirm that motion does affect the output of CCTA, there arises a need to classify how different parts of the coronary tree move during the scan. There also arises the need to find and compare the degree of motion among different patient population.

There is another inherent aim that develop when we talk about motion of these arteries. We would also want to affirm if the arteries stopped moving, at least for some given interval during a heartbeat. If it does stop, what is the duration for which it comes to a halt, because that particular interval can be put into use for CT applications.

Combining these major aims for this particular problem, we devised a method that is explained in the next section.

### **4.3 Methods**

For the purpose of studying the motion in actual coronaries, we used the data from a pool of cath data of patients provided by ‘Heartflow Inc’. Heartflow Inc. is a company based out of Redwood City, CA which works on improving the non-invasive diagnostic techniques in healthcare. We have the data of invasive catheterization done in four patients. They were anonymously renamed as Case\_001 through Case\_004. We had images of the invasive angiography done on them at different angles. That was denoted by the sub-numbering done as, for instance Case\_003(1) and so on, for all the five cases.

The general outline was to create a profile of velocity or a velocity map for each of the segments of the coronary tree. A coronary tree is the network of all the coronary arteries that feed the heart tissue, and because of its resemblance to a tree, it gets its name.

The data that we have for each case, at each angle of acquisition consists of a series of DICOM files over multiple heartbeats. The images were recorded at a frame of 1 frame per 66 milli-seconds. For each case, we select one heartbeat interval, also known as the R-R interval. For doing that we used another analysis software, known as OsiriX. It fully supports the DICOM standard for an easy integration in the workflow environment and is an open platform for development of processing tools.

After gathering a series of images that account for one R-R interval, we used an outsourced non-rigid registration algorithm in MATLAB, to map each frame with its

immediate succeeding frame, and get a transformation field that gives the instantaneous motion of that particular frame in consideration. This registration was performed over all the frames present in our input and a resultant four-dimensional matrix was created that contained the velocity (motion) of each pixel point in each frame, after scaling it to be in the mm/s format. (Two dimensions for the 2-D image, one for the series of frames and one for the velocity values). The results of this algorithm were .avi format videos, which can't be shared in the text, but the screenshots at few time frames can be found in the result section below. The original videos are available as a digital attachment with this thesis.

Another key result that was needed to be obtained was how does different segments in each coronary tree (or case) moved. The different segments are physiologically defined and are shown in the figure below.

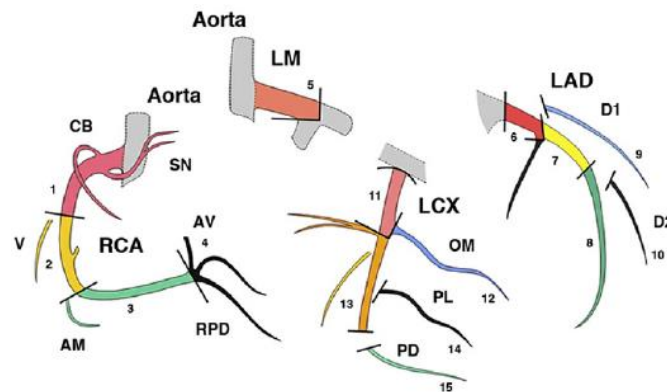


**Figure 4.1 Labeled coronary segments per AHA**

To incorporate this, another algorithm was implemented as follows. Since, we already have velocity maps of each of the time-frame; among the various segments of the coronary tree as listed in the Figure 4.1 above, the major segments in LAD, LCX and RCA were chosen. These were chosen because of their physiological significance in feeding the heart muscle. To create a velocity profile for each of the selected segments, a segmentation

tool was used, where we selected the segment of interest and plotted the maximum velocity in that segment with respect to the time-frame that it belongs to.

The plots for the same are shown in the results section.

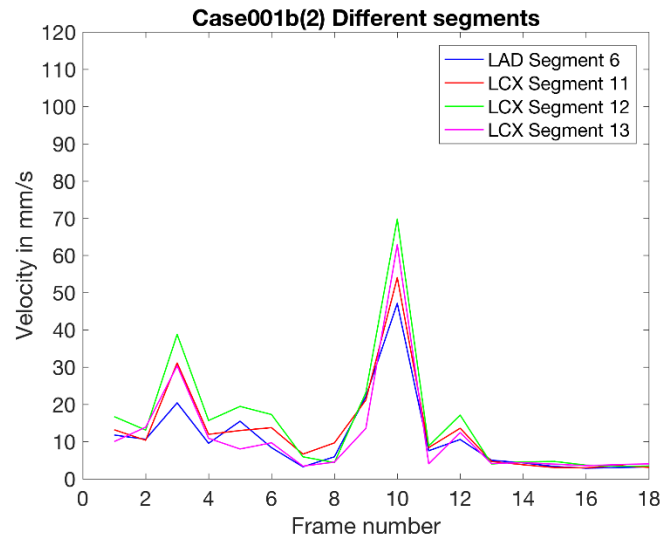


**Figure 4.2 Velocity profile of various coronary segments along the R-R frames**

Another inference that could be made from this study is how each segment behaves in different people. To affirm this, we created velocity maps of various segments in different cases and plotted them on the same axes. This was additionally done to find out if the arteries have some trend in coming to rest over the entire R-R interval, so that we can make a generalization while scanning the artery of interest. The results for this section of study are also included in the section 4.4.

#### 4.4 Results

The movies that track the velocity and relative position of the coronary segments are available as digital attachments (in supplementary files) with this thesis. Figure 4.3 shows a screenshot from one of those movies, Figure 4.3(a) showing the relative position of the

coronary artery (in black) with respect to the first frame (end diastole, in white); and Figure 4.3(b) shows the color coded velocity values, for all the segments:

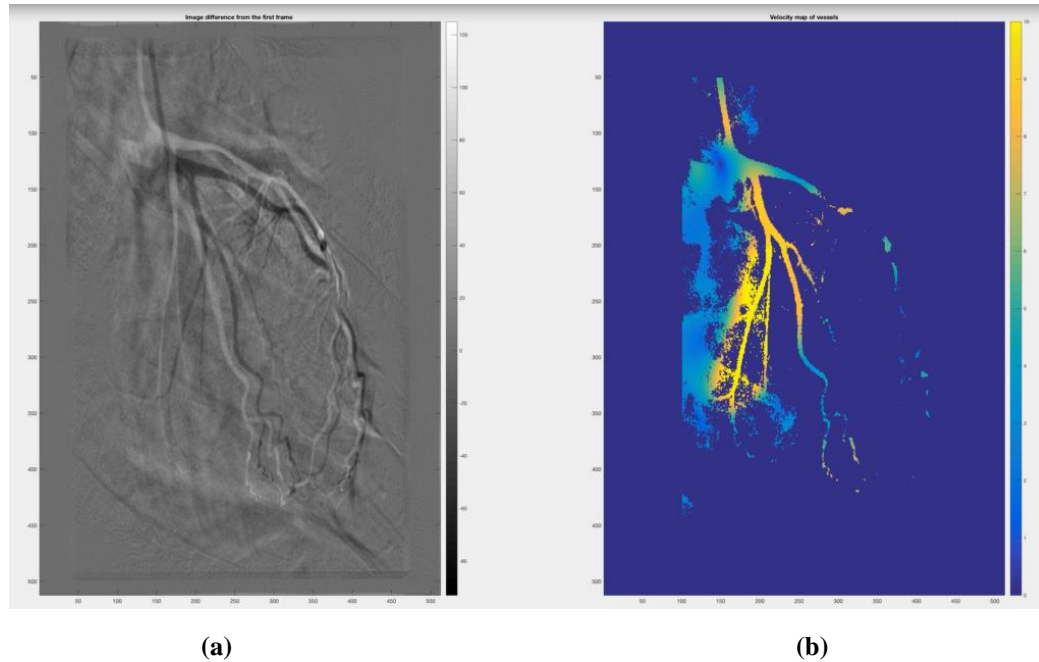


**Figure 4.3 (a) Relative position of coronary tree at a certain frame in R-R interval with respect to frame 1 of R-R interval (end diastole) (b) Color coded velocity value at a certain frame in R-R interval**

The second part of study involved recording velocity as a function of time points in the R-R interval. Figure 4.4 through Figure 4.9 show that velocity profile, each figure corresponding to an individual case, with different segments of the coronary tree.

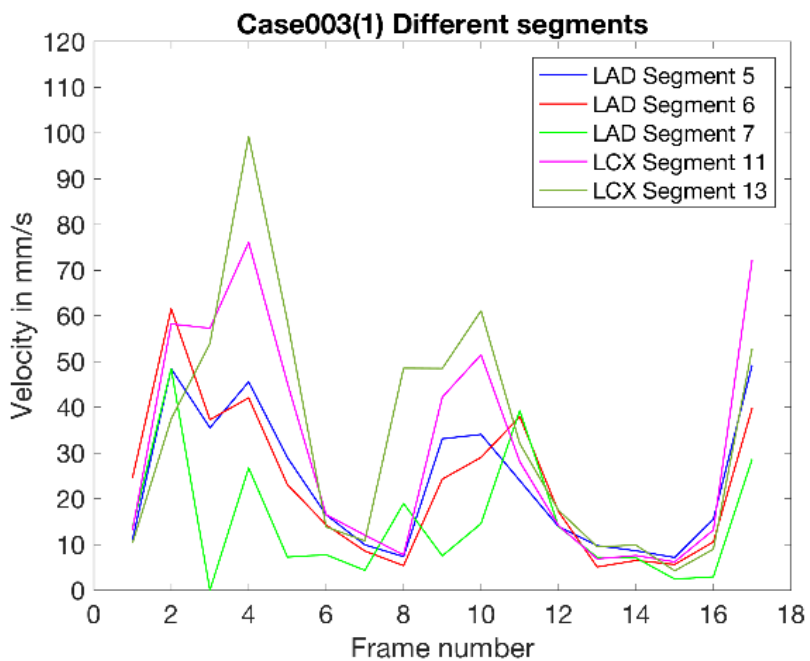


**Figure 4.4** Velocity profile of various coronary segments for Case003(1) along the R-R frames

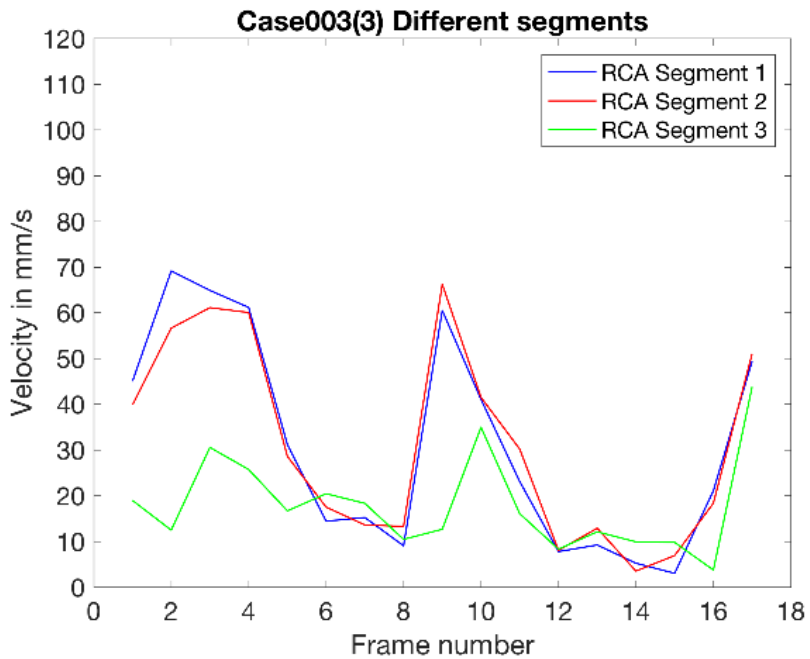


**Figure 4.5** Velocity profile of various coronary segments for Case003(3) along the R-R frames

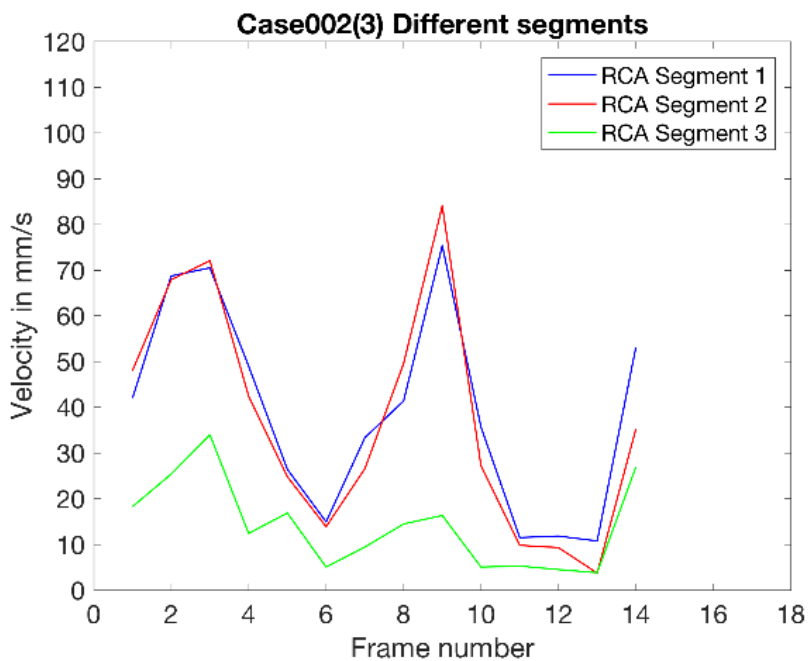


**Figure 4.6** Velocity profile of various coronary segments for Case002(3) along the R-R frames

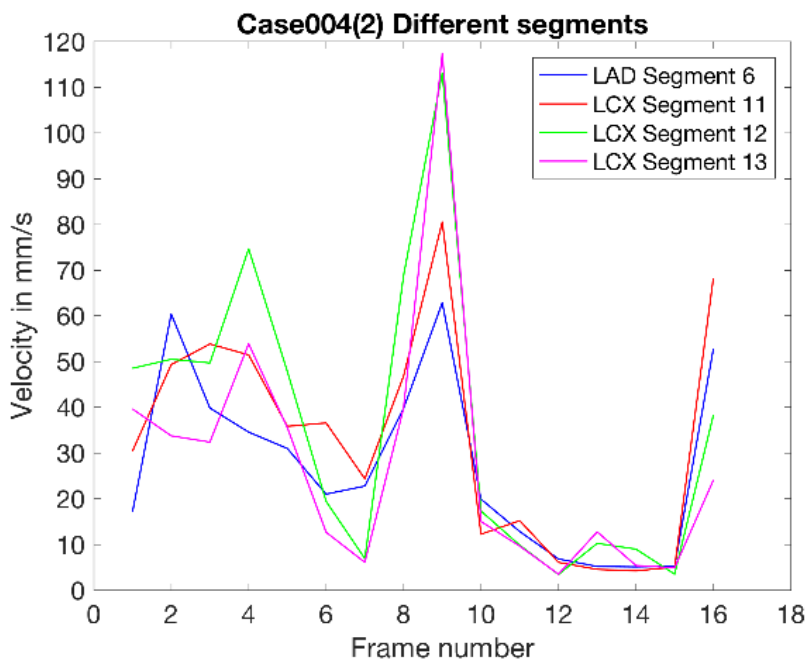


**Figure 4.7** Velocity profile of various coronary segments for Case004(2) along the R-R frames

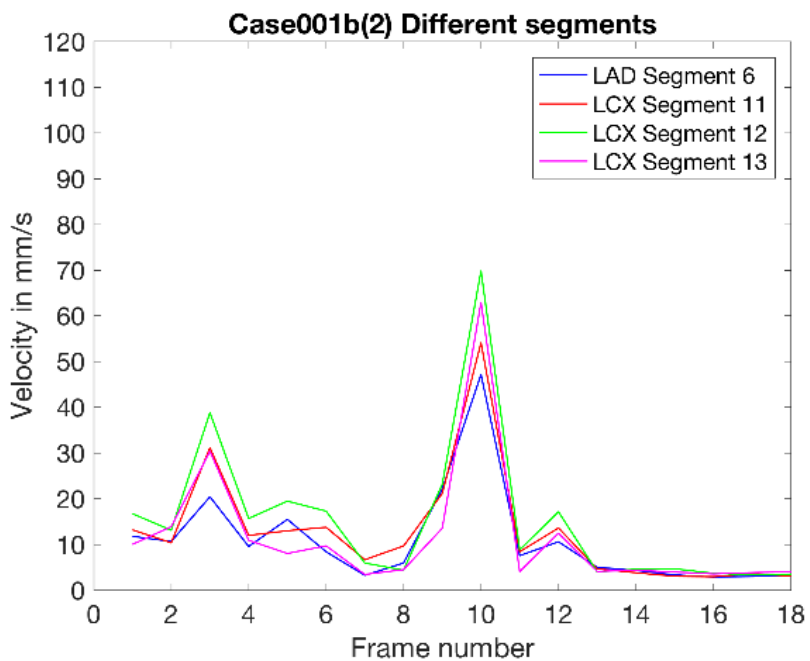


**Figure 4.8** Velocity profile of various coronary segments for Case001b(2) along the R-R frames

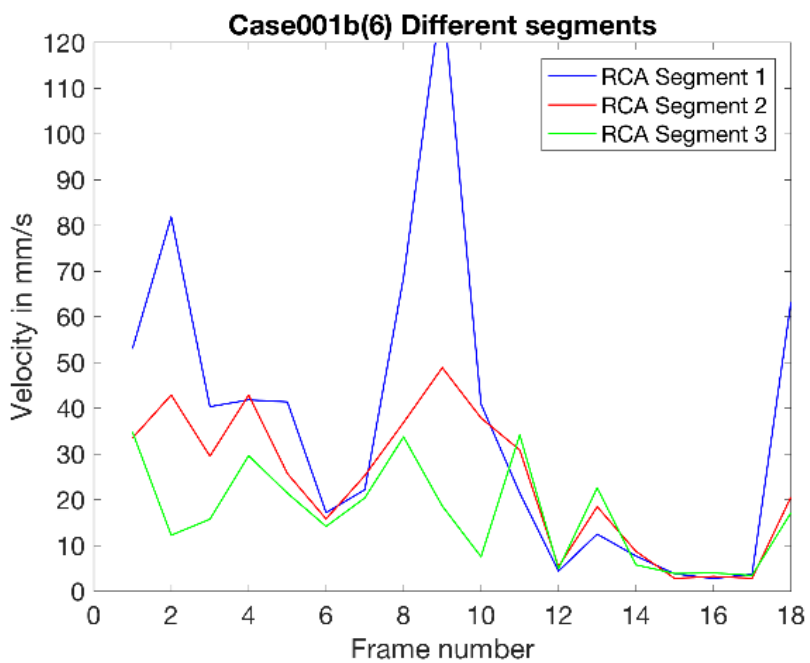


**Figure 4.9** Velocity profile of various coronary segments for Case001b(6) along the R-R frames

Figure 4.10 through Figure 4.13 contain the plots that show the velocity of a particular coronary segment with respect to frame in R-R interval, in different subjects:

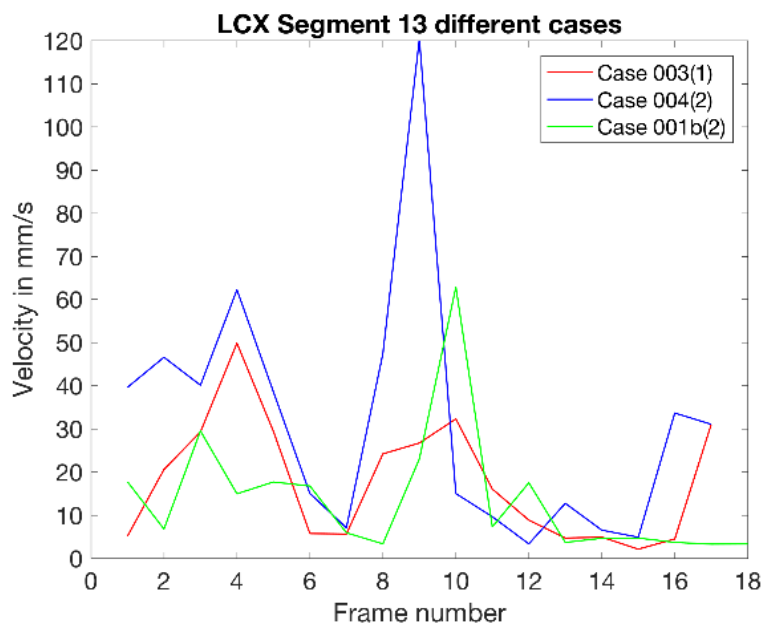


**Figure 4.10** Velocity profile of LCX distal segment along the R-R frames in various

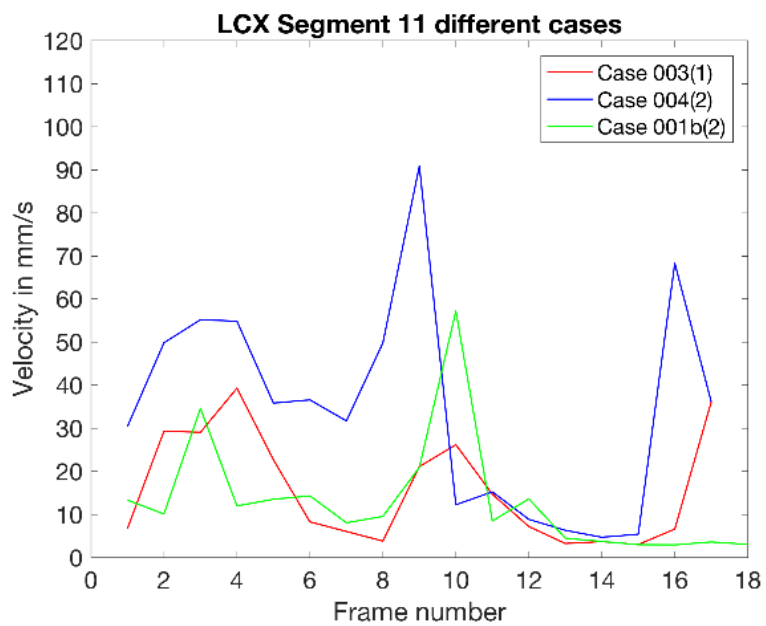


**Figure 4.11** Velocity profile of LCX proximal segment along the R-R frames in various subjects

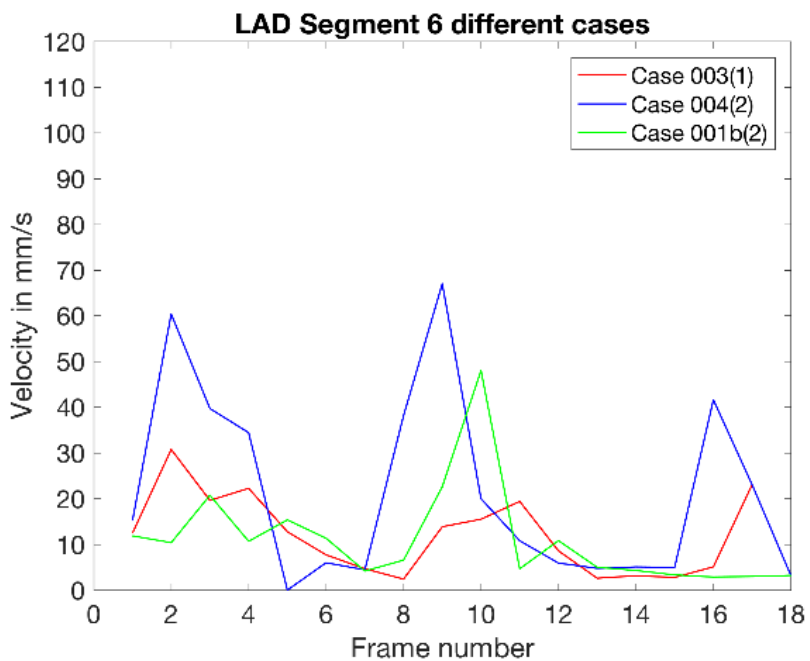


**Figure 4.12 Velocity profile of LAD proximal segment along the R-R frames in various subjects**

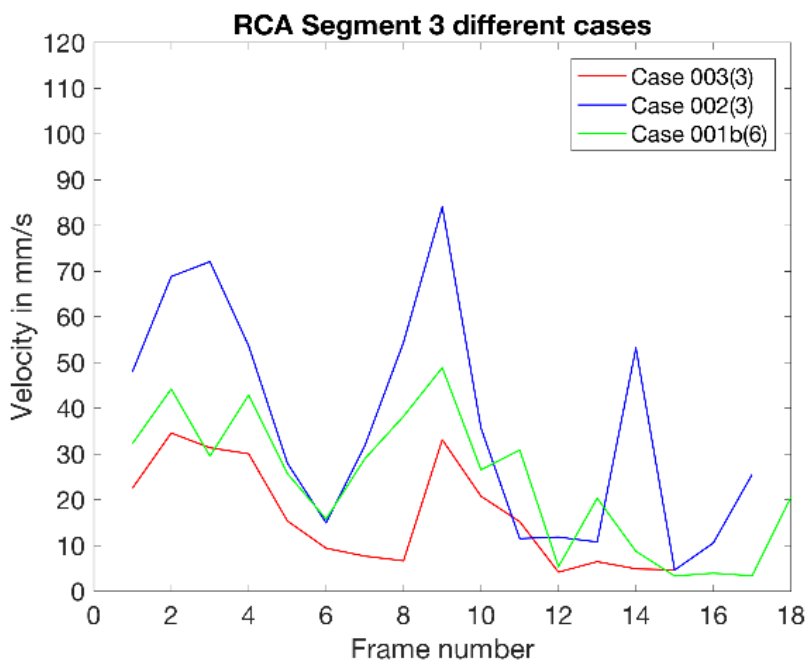


**Figure 4.13 Velocity profile of RCA distal segment along the R-R frames in various subjects**

## 4.5 Conclusion and Discussion

A distribution of the average velocity during diastasis for a total of 22 coronary segments was created, which looks as follows:

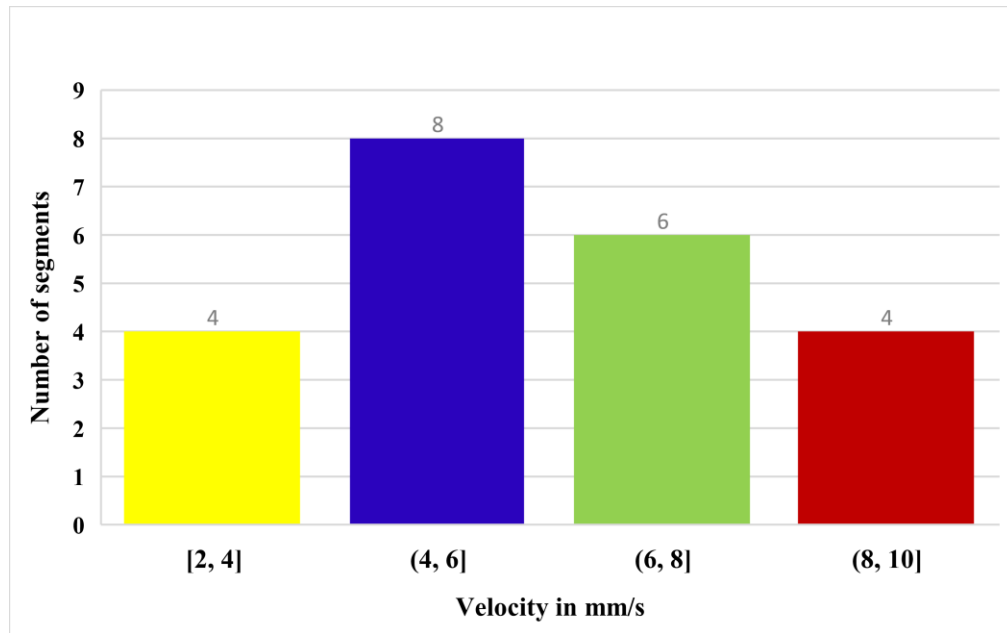


**Figure 4.14 Distribution showing number of segments having various amounts of motion**

Based on this distribution and the velocity plots in the results section 4.4, we could argue that during diastasis, the coronary arteries move at an average velocity of 6 mm/s, and that could be equivalented to a constant velocity motion over the diastasis. Another argument to be made is the average time that these segments stay in diastasis, which could be estimated by the following distribution, concluded according to the data in the results section above:

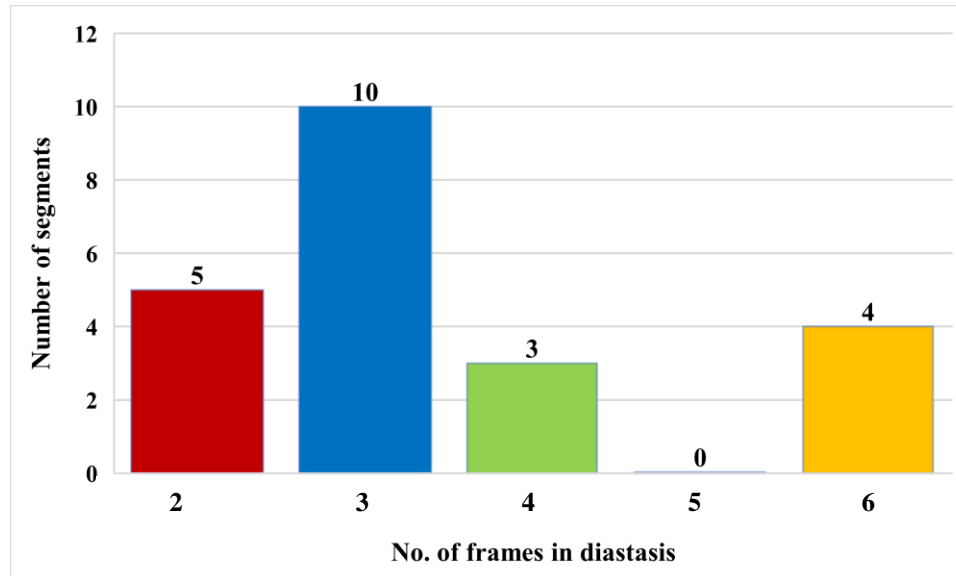


**Figure 4.15 Distribution showing number of segments in various duration of diastasis**

The average number of frames during diastasis can be averaged to three, which is a time-duration of 198 ms (because each frame is 66 ms).

Hence, if we could model the coronary arteries as having a constant velocity over an interval of 198 ms, we could use those frames in R-R interval to do the CCTA, with motion artifacts being the minimum.

Additionally, since the velocities are measured using one view of angiogram, therefore they might not be the highest value of motion happening, but is definitely the minimum velocity of the coronary arteries, and should be a concern that should be addressed.

## CHAPTER 5: SIGNAL INTENSITY CHARACTERIZATION WITH GEOMETRY AND ORIENTATION

### 5.1 Introduction

One of the most important features of an image is its intensity. The varied levels of intensity make the different regions of an image appear differently. Hence, two images of a same object can be perceived differently based on the image gradient that they have.

In case of CT images, the intensity is measured in a scale known as the Hounsfield Unit scale. The Hounsfield scale or CT numbers, named after Sir Godfrey Newbold Hounsfield, is a quantitative scale for describing relative inability of X-rays to pass through a particular material, also known as radiodensity. The Hounsfield units scale is a linear transformation of the original linear attenuation coefficient measurement into one in which the radiodensity of water measured at Standard temperature and Pressure (STP) is defined as zero HU, while the radiodensity of air defined at STP is -1000 HU. Attenuation coefficient defines how easily electromagnetic wave, such as X-ray can penetrate a material. In a voxel (volume element), with average linear attenuation coefficient, the corresponding HU value is given by:

$$HU = 1000 \frac{\mu - \mu_{water}}{\mu_{water} - \mu_{air}}$$

where  $\mu_{water}$  and  $\mu_{air}$  are respectively the linear attenuation coefficients of water and air.

Now that we know what intensity means and what the units are, we can go ahead and start defining the purpose of this study.

## 5.2 Purpose

The main aim of this study was to characterize the signal intensity, as measured in HU, as it pertains to the geometry of the coronary vessels. The motivation behind this study was the simulation study done by Dr. Francisco Contijoch for an abstract submitted in MedPhysics [46]. The study included designing of a computer simulated phantom of cross section of the vessels having diameter ranging from 0.3 mm to 2 mm and running an algorithm that mimics the actual projection mechanism and eventually back projection, that happens in a standard clinical CT scanner, thereby resulting in a ‘CT image’ of corresponding phantom vessels.

The paper listed out results of the variation of intensity with respect to the diameter size, considering the CT scanner specifications, such as resolution, spot size, etc. alongside.

Our study aimed at affirming similar results in a custom made physical phantom and a set of real patient data, to characterize the impact of vessel geometry, hence the diameter size on the resultant HU intensity in the CT image.

## 5.3 Methods

For the effectiveness of this study, a physical phantom was designed. The phantom was made from acrylic and had through holes of varied diameters ranging from 0.4 mm to 3 mm drilled in it using the high-precision drills at one of the engineering labs at UC San Diego. This phantom was then scanned in a GE VCT 64- slice CT scanner at UC San Diego Jacobs Medical Center, and the CT images were recorded to be analyzed later.

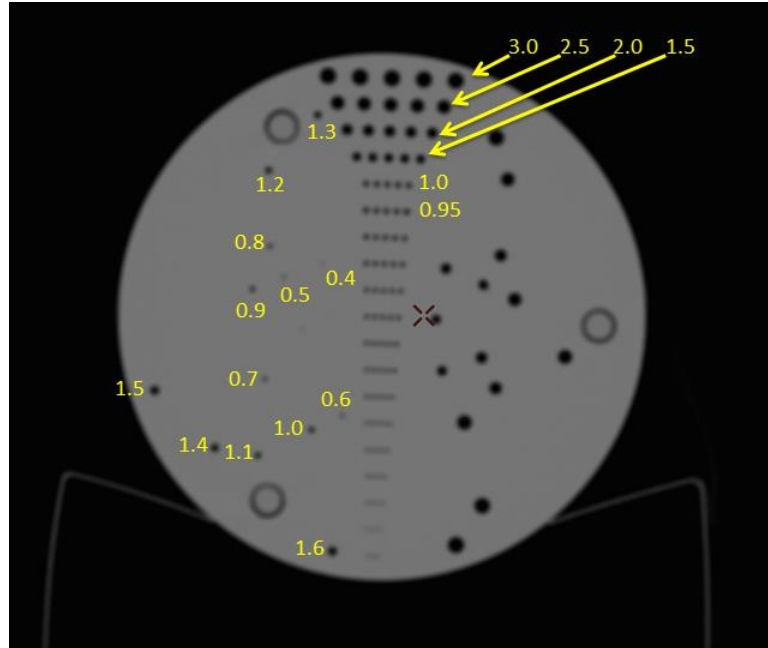


**Figure 5.1 CT image of the physical phantom with holes of different diameter sizes (in mm), marked**

Once we had the corresponding CT image, a technique similar to what was used in the simulation study[46] was used to infer the HU intensity values of the subsequent diameter range. A FWHM (Full Width Half Maximum) approach was used to measure the diameter size as observed in the image, and the intensity value was recorded as the maximum HU value in a defined ROI around the cross sectional vessel of interest [47].

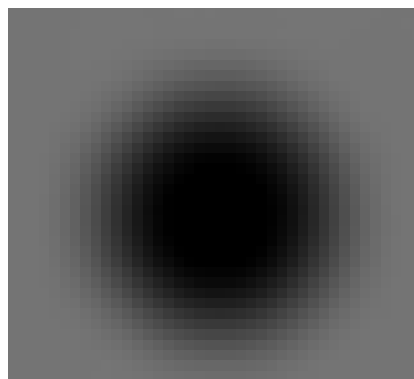


**Figure 5.2 Cropped view of diameter hole sized 3.5 mm, as observed in the CT scan**

A plot of observed diameter v/s intensity was then plotted. Also, a plot of true diameter v/s intensity was plotted.

After the results were obtained for the phantom, and since they matched the simulation study results, the same operation of relating signal intensity to diameter was performed on a dataset of human CCTA. The dataset was obtained from National Institutes of Health (NIH) and was anonymized before being available for use for analysis purposes.

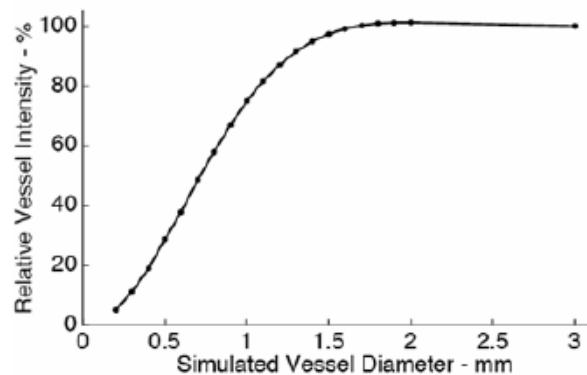


**Figure 5.3 Relative intensity with respect to diameter per digital simulation [46]**

After pre-analysis of the CT images for their usability for the analysis, using OsiriX, a total of seven patient data sets were chosen. We had the CT images for the entire heart. Since we were concerned about the coronary CT images, we used a software called QAngio (Medis Medical Imaging systems, Raleigh, NC).

The data set we required as an input had to be a set of different vessels of varied sizes. Also, to match the clinical standards, we decided to perform the study on a per-vessel basis. This included carrying out the study on three major vessels for each patient dataset. The three major vessels, as mentioned above are Left Anterior Descending Artery (LAD), Left Circumflex Artery (LCX) and Right Coronary Artery (RCA). These three were chosen

because they have the major role in feeding the myocardium. If there is a lesion in any of these, it is far more significant than having lesion in one of the other vessels that branch out from these three, for instance, Diagonal branch and Obtuse Marginal, etc.

The protocol to perform pre-processing on the CT images, for each of the vessel was as follows:

The series of DICOM files was loaded in to the QAngio software. DICOM is a format in which the images are stored as a result of reconstruction procedure in a clinical CT scanner. The software has an application which detects the coronary tree from those CT images and generates an image that consists of just the coronary tree and gets rid of other parts of the heart tissue. The resulting coronary tree has each of the vessel labelled, as shown below.

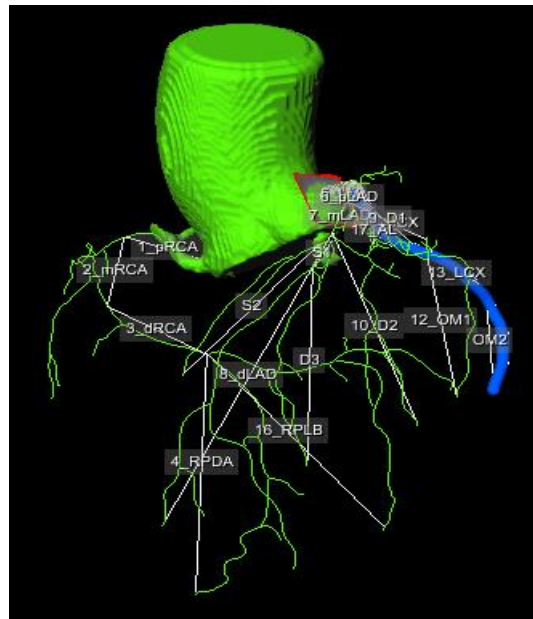


**Figure 5.4 Coronary tree generated by Medis QAngio with labelled segments**

Next, we choose the artery of interest, and QAngio displays that in a longitudinal, as well as in a transverse (cross-sectional) view. There is a slider which lets us slide down the artery in the longitudinal view and displays the corresponding cross-sectional view.

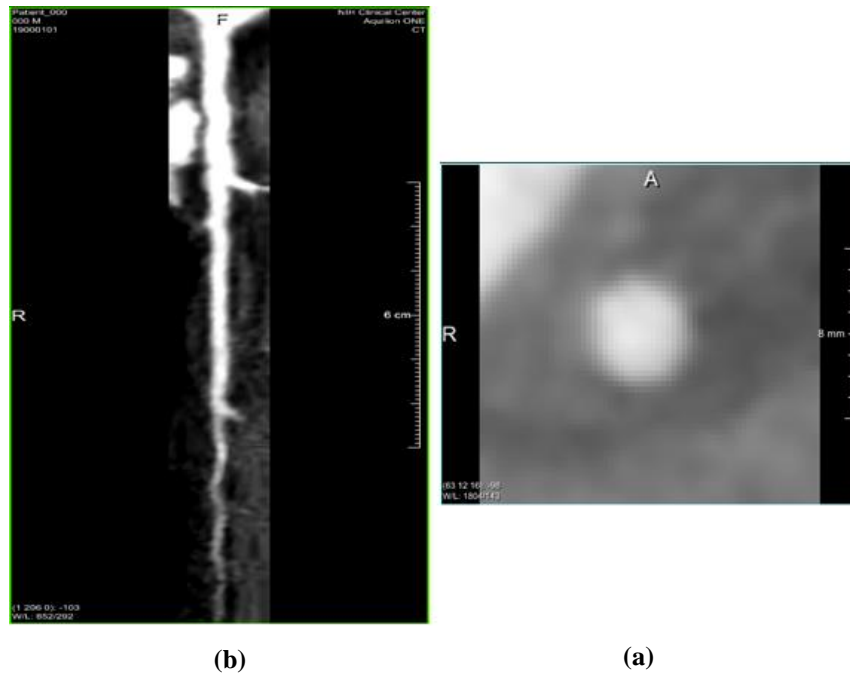


**Figure 5.5 (a) Longitudinal view of a coronary vessel in Medis QAngio  
(b) Transverse view of one slice in the corresponding vessel in (a)**

Now, the prime objective was to obtain cross-sectional images of different diameter sizes, hence the cross-section view for different diameter sizes, ranging from proximal artery to the distal artery were saved in a directory. This method was repeated on all the three above mentioned arteries for all the seven patient data sets mentioned before.

Each vessel for each patient formed a separate input of the analyses and the following algorithm was thence implemented to estimate the intensity value (in HU) and measure the diameter.

To estimate the HU value of each diameter size vessel, the algorithm calculates the maximum intensity value in the manually cropped ROI, and returns a HU value after scaling it from the units used by Medis QAngio.

To measure the vessel diameter and shape, the full-width half maximum (FWHM) region of the vessel was identified using the signal intensity at the vessel center as the maximum. The diameter was calculated as the major axis of an ellipse fit to the full-width half maximum contour.

The above two steps were performed for each of the diameter size and then plots were created to show a relevance between the intensity values and diameter size.

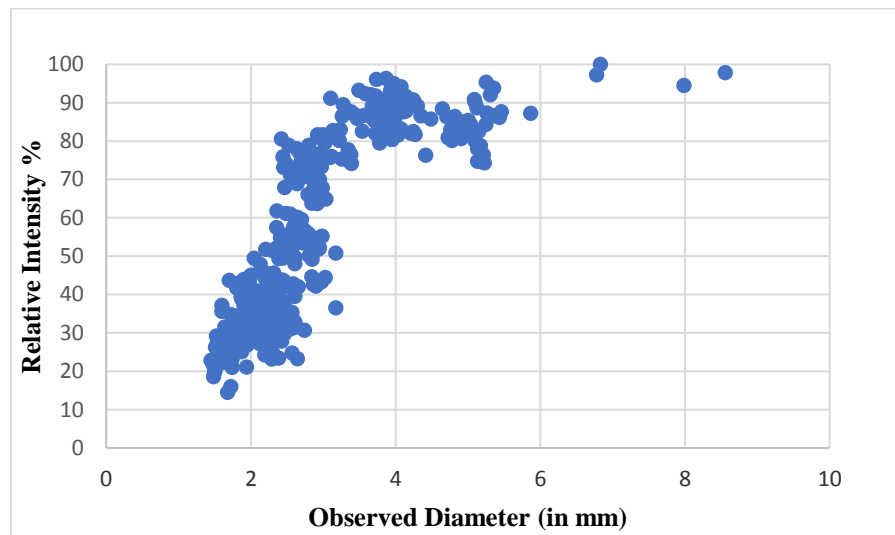


**Figure 5.6 Relative Intensity with respect to observed diameter in LAD of a human heart**

The above plot was obtained as a result of analysis done on a patient coronary data for a particular phase in R-R cycle for LAD, in QAngio, and creating a relative intensity map with respect to the measured diameter. In the results section 5.4 below, similar plots containing relative intensity information with respect to the observed diameter are presented, after taking the FWHM measurements.

## 5.4 Results

The measured intensity v/s diameter for physical phantom is shown below:

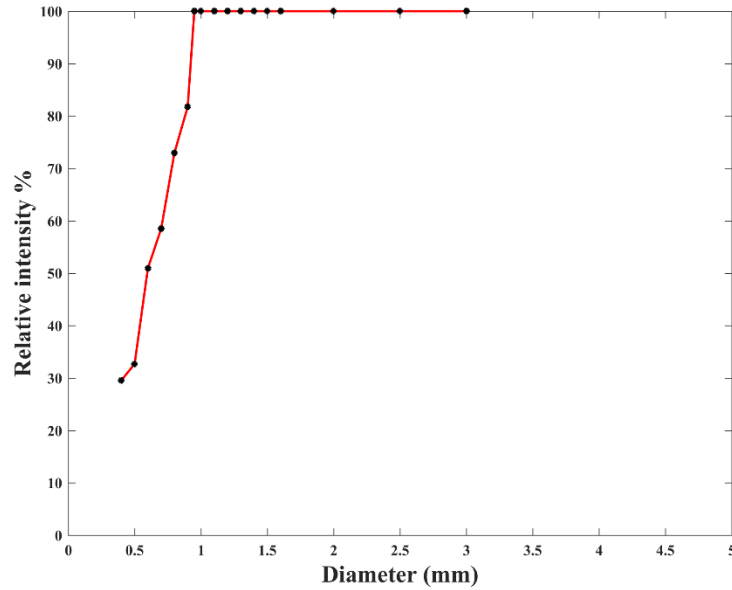


**Figure 5.7 Relative Intensity with respect to diameter values in phantom**

This result confirmed the simulation results reported in the abstract [46]; thus, showing a steep drop in the intensity values for diameter ranges smaller than 1.5 mm.

The results obtained from patient CCTA data for different coronary arteries are shown below; with the anonymized identity of the patient and the vessel name in the figure details, and the phase of R-R in the legend:

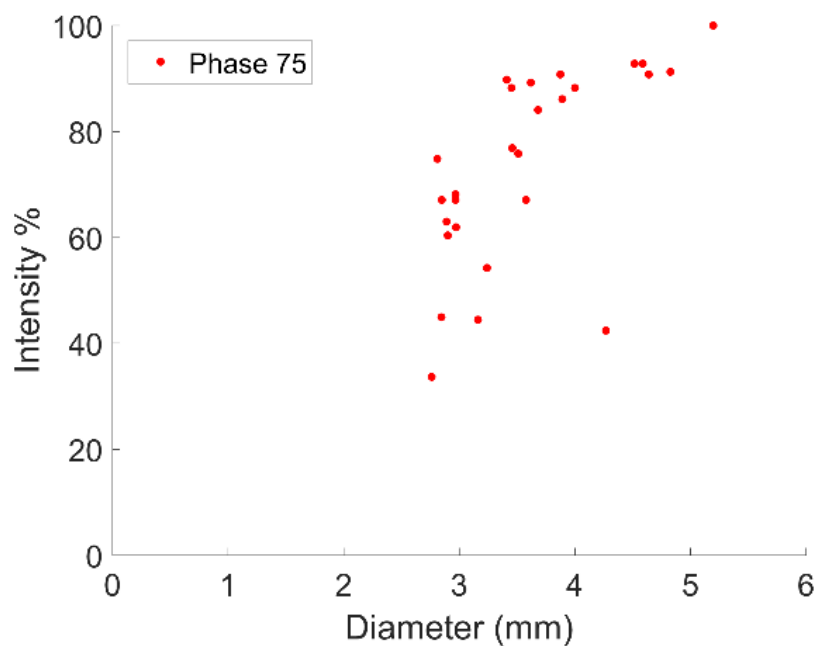


**Figure 5.8 Relative intensity with respect to observed diameter in LAD of Patient 000**

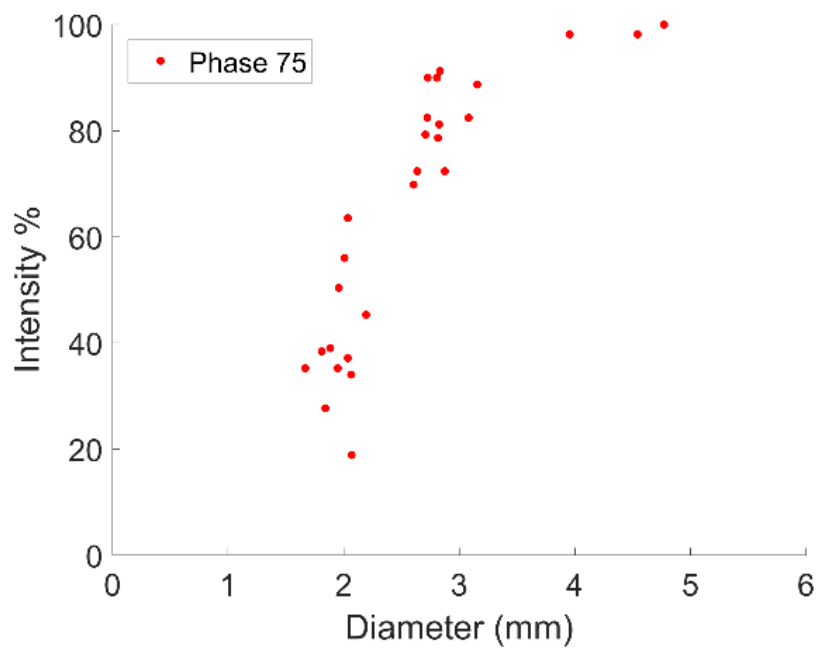


**Figure 5.9 Relative intensity with respect to observed diameter in LCX of Patient 000**

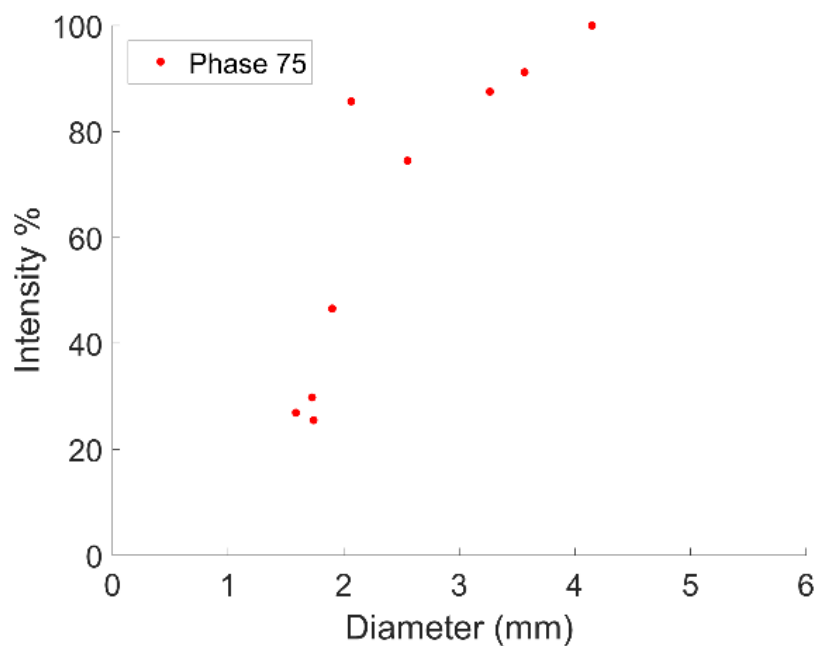


**Figure 5.10** Relative intensity with respect to observed diameter in LAD of Patient 005

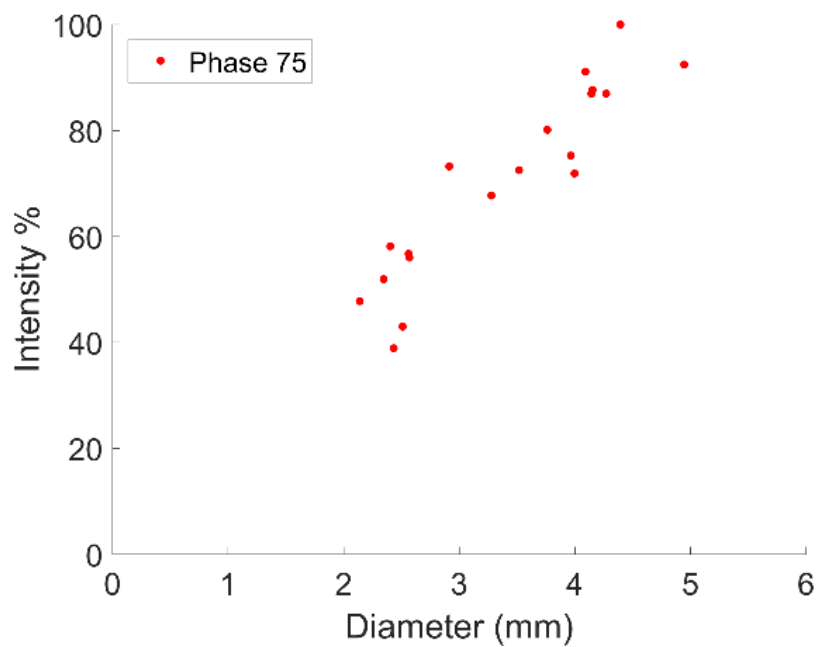


**Figure 5.11** Relative intensity with respect to observed diameter in LCX of Patient 020 (75% of R-R)

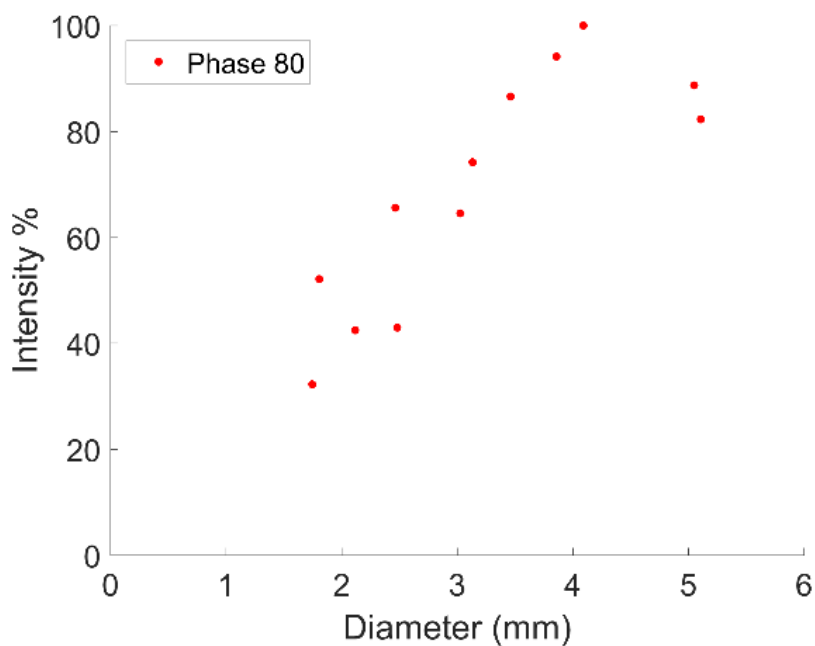


**Figure 5.12** Relative intensity with respect to observed diameter in LCX of Patient 020(80% of R-R)

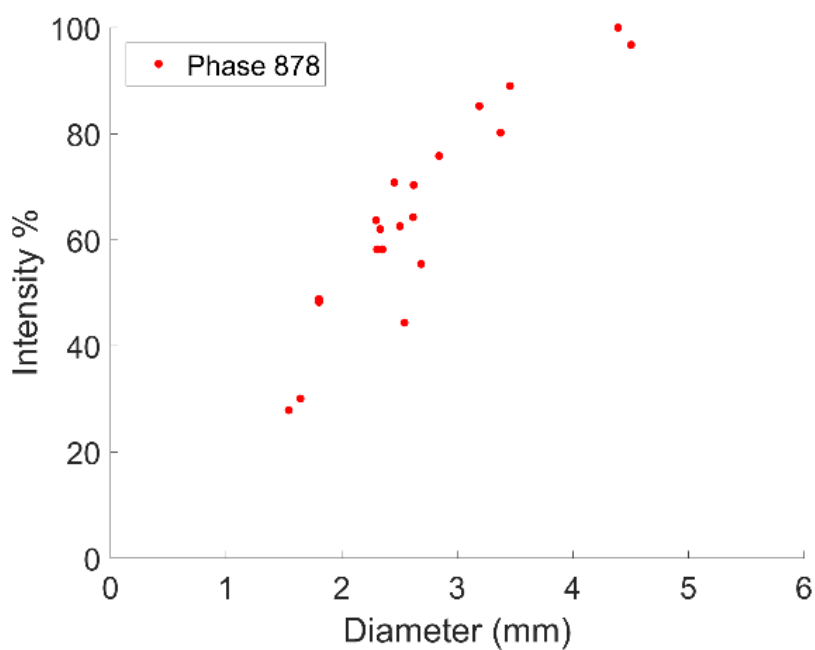


**Figure 5.13** Relative intensity with respect to observed diameter in LCX of Patient 023

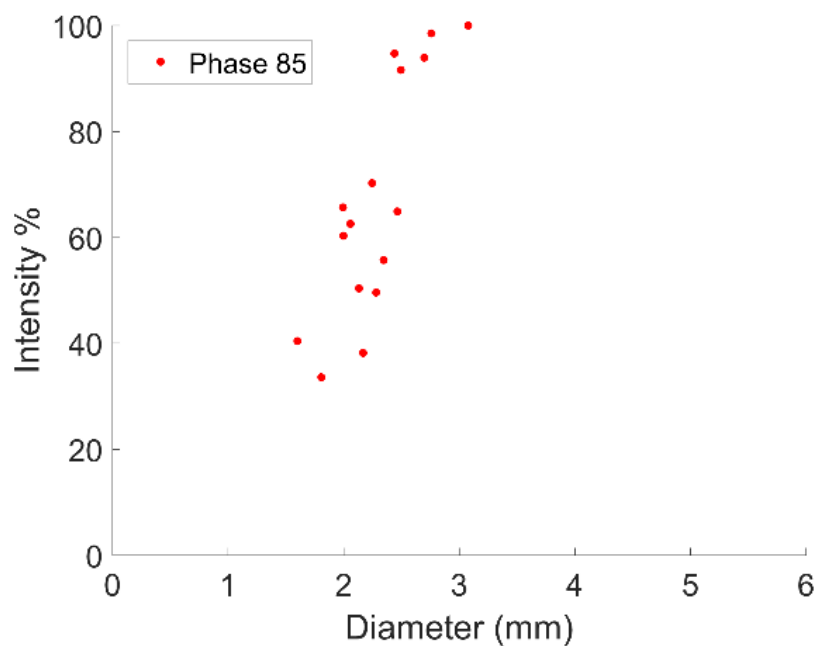


**Figure 5.14** Relative intensity with respect to observed diameter in RCA of Patient 023

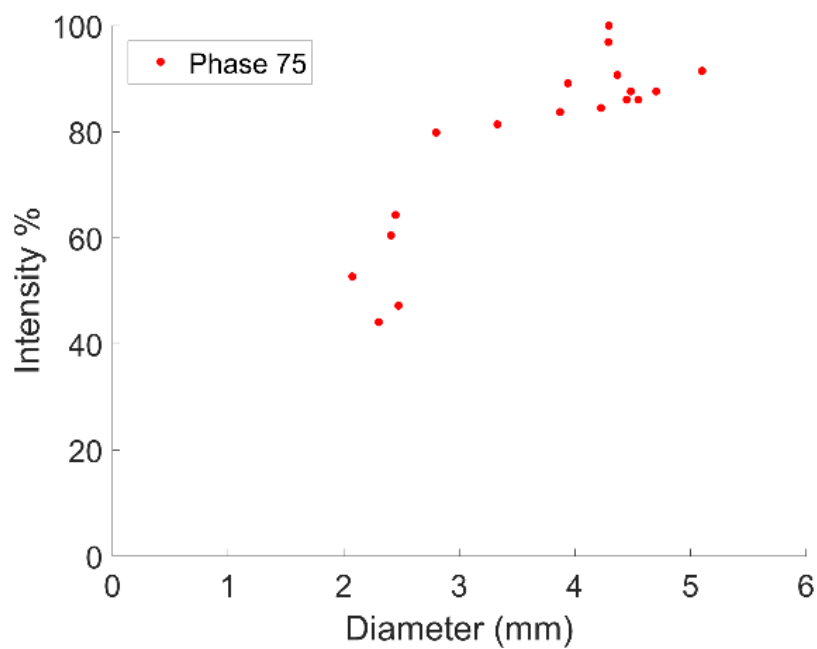


**Figure 5.15** Relative intensity with respect to observed diameter in LCX of Patient 026

Using QAngio software, relative intensities were recorded against the observed diameter, which is plotted in Figure 5.16, below

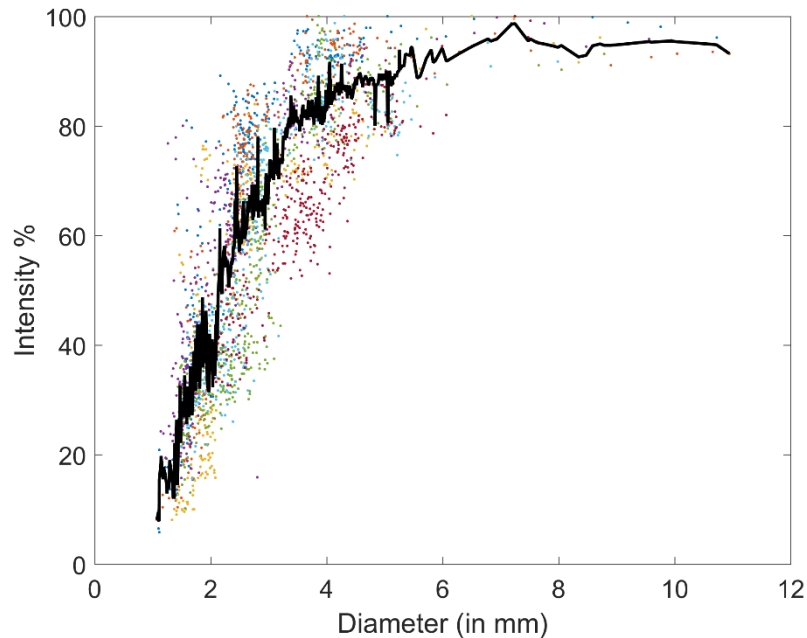


**Figure 5.16 Relative intensity with respect to observed diameter for entire patient dataset (average trend in black)**

Using this plot as the basis of intensity calculations based on commercially available software, we could gather an estimate of the signal to noise ratio required to get ‘good’ intensity measurements, to be around 4 dB. While this is not a perfect estimation of the given quantity, but this could be used as a control for the later studies.

## 5.5 Conclusion and Discussion

As the diameter decreases, the intensity value drops and after a particular threshold value of diameter, which largely depends on the scanner resolution of CT, the diameter appears the same size, only its intensity starts to decrease.

This finding is important because in case of lesion, the effective diameter size of a vessel decreases at the point of lesion and as suggested above, we should observe a dip in the intensity at that point. Hence, it adds an additional flag to support the diagnosis of a lesion at that point, rather than just being a visual diagnosis, which can be overlooked by some radiologists due lack of experience.

Another important finding that suggests that the observed diameter remains same but the intensity drops if the diameter is below a threshold value, makes us want to believe that in real diagnosis scenario, if there is a lesion that causes the artery to get way thinner beyond that threshold, there is no way we could tell the actual diameter of that artery, which raises some concern about the credibility of making visual inference.

## **CHAPTER 6: SIGNAL INTENSITY CHARACTERIZATION WITH CARDIAC MOTION**

### **6.1 Introduction**

We have already talked about the importance of intensity values for an image, particularly CT image, for our interest. CT scan methods were originally used for brain imaging majorly and those used to give outstanding results because of the high quality of CT itself, and the fact that brain does not move during its entire scan time. But, the issue while doing a cardiac scan is that the heart is beating during the scan and this causes some artifacts. Imaging a coronary artery results in even more dire consequences with motion as they are very small in dimension and a small error greatly affects the resulting image.

This effect was also studied as a part of the simulations done by Dr. Contijoch [46], which was the motivation behind the following study.

### **6.2 Purpose**

The results suggested by Dr. Contijoch's simulations [46] showed that the intensity values are affected by the varied degrees of motion in the coronary arteries during the scan. Coronary CTA is usually performed during diastasis, which occurs approximately 75% through the R-R interval. During that time, for most patients, the coronary vessels are at their most quiescent; however, because modern CTA image resolution is so high, even a small submillimeter drift of the vessel can modify the signal in the vessel. These simulation results led to the study of motion effects in the physical phantom and real patient data. This

study was done to prove that there might be an overestimation of vessel diameter because moving coronaries might result in an image that is apparent.

### 6.3 Methods

The same physical phantom that was used in the previous study was used for this study as well. Since, we had to create the motion in the phantom to mimic the cardiac motion, we used an NRT 100 motor actuator (Thorlabs, Newton, NJ). It is a platform as shown in the Figure 6.1 which can produce small motions ranging from 0.5 mm/s to few tens of millimeters/s with sub-micron precision.



**Figure 6.1 NRT 100 motor from Thorlabs**

We programmed the motor platform to move at four different velocities, i.e. 2 mm/s, 4 mm/s, 6 mm/s, and 8 mm/s; using a software called APT, that configures the motor and was able to communicate with a Windows desktop using a BSC 202 Motor Controller (Thorlabs, Newton, NJ).

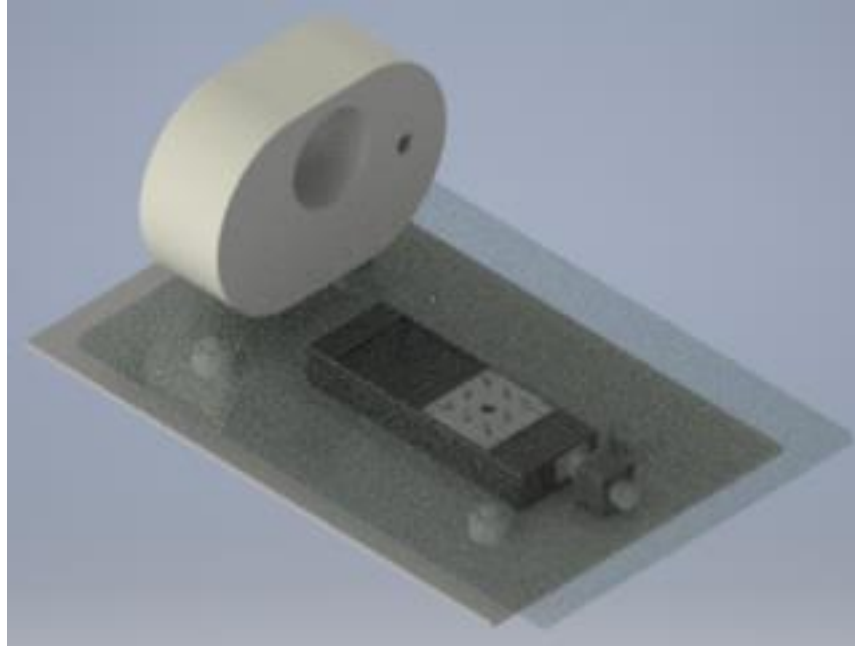


**Figure 6.2 Set up of phantom and motor assembly to scan for studying motion effects on CT image**

For each of the four different velocity values and for a stationary phantom, CT scans were performed on the phantom, using a Toshiba 64 slice CT scanner at UC San Diego Jacobs Medical Center. The images for each case were then recorded and fed to OsiriX for pre-analysis before further processing was done. The scans were performed multiple times to get the best images as this study would affect the way we proceed with patient data. Once we had the images, the images were fed to an algorithm that did the following:

The algorithm finds the intensity value of each of the respective diameter size, by returning the maximum HU value from a cropped ROI around the ‘vessel’. The diameter of the ‘vessel’ was found using the same FWHM approach as in the previous study. This was done for a range of diameter sizes in stationary and the four different velocity cases,

as mentioned earlier. Intensity v/s diameter plots were plotted for each of the case, as shown in the result section 6.4.

After performing the study on phantom data, the set of patient data used in previous study (NIH data) was recovered and analysis was done. Since the motion was unknown in the real patient dataset, the most stationary frame was chosen during pre-analysis done using OsiriX, and data from the successive two frames were selected as being 'in motion'. The intensity values and diameter measurements were then made on this data using the transverse views from QAngio, as done in the previous chapter's study. Consecutively, plots were drawn between intensity values and observed diameter from all the different frames that were taken into account, for each of the patient set.

#### **6.4 Results**

Following trend was observed in the intensity values of true diameter over the 4 different velocities imparted by the motor:

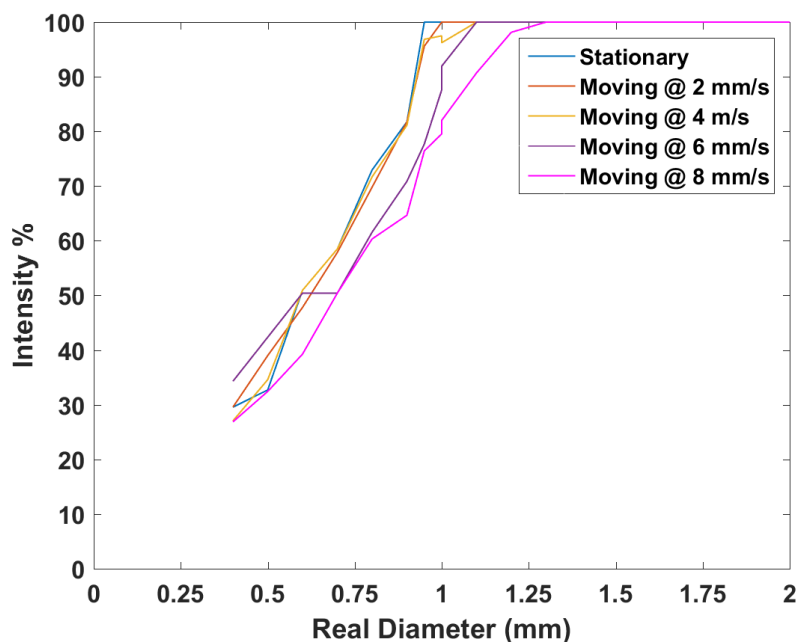


Figure 6.3 Plot showing the trend of intensity values with real diameter values

This matched closely with the digital simulation results, which were:

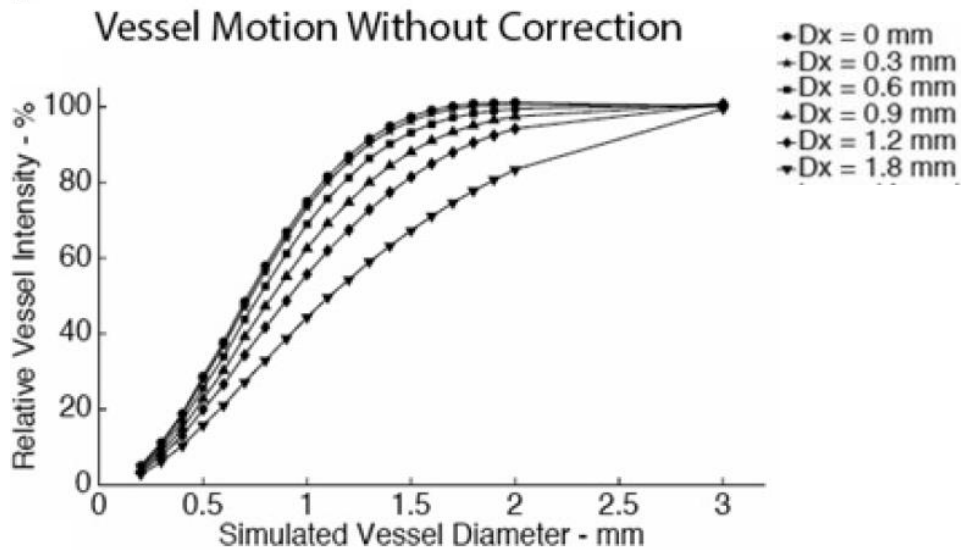
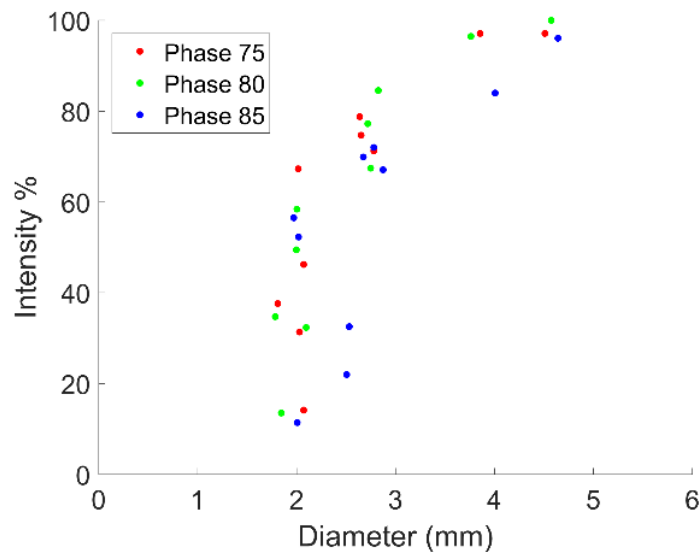


Figure 6.4 Plot showing the trend of intensity values using digital phantom [46]

Although, the results with using physical phantom didn't show as much variation in intensity values with changing velocity as it did in digital simulation, because of the

better control of CT scanner parameters, specifically gantry angle, in digital simulations, but we could still confirm the right shift in the curve with increasing velocity.

The study for motion effects on the patient data was expected to give inconsistent results because of various limitations of the dataset itself, such as not knowing the position of the slice of the vessel in z-direction, which led to improper intensity values, hence disrupting the possibility to capture a trend of the intensity values with diameter. As expected, the results were not as consistent as they were in the phantom study, they are shown below because they give a hint of the possible variation that occurs in intensity values with motion.



**Figure 6.5 Plot showing the trend of intensity values in LAD of Patient 000 at 75%, 80% and 85<sup>th</sup> time frame during R-R interval**

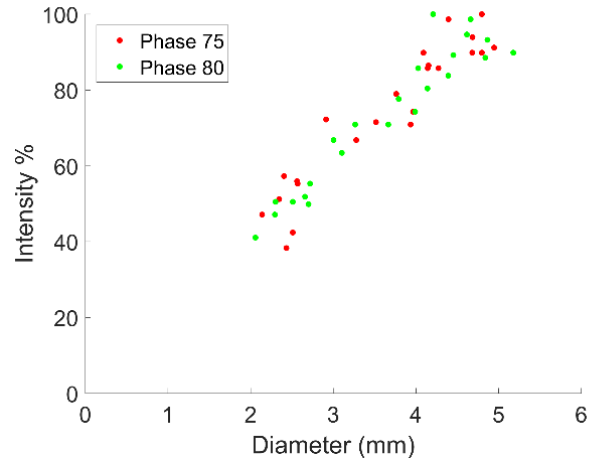


**Figure 6.6 Plot showing the trend of intensity values in LCX of Patient 020 at 75% and 80<sup>th</sup> time frame during R-R interval**

## 6.5 Conclusion and Discussion

An important finding that was observed is that the results closely matched the original simulation results, hence verifying Dr. Contijoch's computer simulation. Secondly, we observed that due to the small motion of coronary arteries, the diameter values that were observed were rather apparent and tend to increase with increasing motion. Having said that, it suggests that if diagnosis is made overlooking the motion effects, there might be a case when an actual lesion might go unnoticed because it would have appeared as a bigger vessel size in the scan image due to motion.

Therefore, there is a need to keep in mind that motion of heart (which is unavoidable) can cause changes in the appearance of the CCTA images and that this should be corrected. There is a need to correct the effect of motion and produce CT images that reflects the true insides of the heart cavity and not a motion corrupt image.

## CHAPTER 7: LIMITATIONS

While there have been significant results derived from this study, there still remain some limitations in the methods that were applied. The velocity profile with respect to frames over the R-R interval require a study in the different views combined as one result. Since each angiogram shows the view of the cardiac phase from different angles and each orientation would return different velocity value, there is a need to take all that into account to model the velocity measurement. The method still requires manual pre-processing, like choosing the specific number of frames from a large range of frames over multiple heartbeats, which makes it less efficient. Also, there is a movement in the detector plane during angiography, which makes most of the frames unsuitable for study. This limitation is due to the fact that the data used was not recorded for this particular study, but was freely available as independent angiogram data. Hence, for a detailed and proper analysis, we require carefully done angiographic data.

In the intensity v/s diameter study, the phantom data gives smooth results, because of evenly spaced orifices made in careful supervision in mechanical labs. However, the results of the patient study have considerable noise due to their non-uniform nature, although we could still confirm the trend of our intensity levels dropping. The other limitations include unknown gantry angles for the recorded data, which might have caused apparent shift in intensity levels and the observed diameter values.

## **CHAPTER 8: FUTURE WORK**

The next steps after looking at the results of this study would be to create an apt quantitative velocity model of the coronary motion during diastasis. This would provide us with an initial mechanism to proceed to motion correction of the CT images corrupted by motion artifacts. Another preliminary future step would be to model the intensity and diameter relationship independent of scanner parameters to get a more objective analysis of actual patient data. This could involve modelling studies on 3D printed coronary trees that would be a close approximation to the actual human data. The inclusion of motion correction in the CCTA images will provide the clinicians with a better way of diagnosis of atherosclerosis and hence reduce the false positives which will greatly reduce the unnecessary invasive catheterization.

## REFERENCES

- [1] Porta, M. D. Rienzo, N. Wessel and J. Kurths, "Addressing the complexity of cardiovascular regulation A", *Philosophical Transactions of the Royal Society*, vol. 367, pp. 1215–1218, 2009.
- [2] G. J. Tortora and S. R. Grabowski, "The cardiovascular system: The heart", in *Principles of Anatomy and Physiology*, pp. 659-695, 2003.
- [3] "The World Health Report - changing history," World Health Organization, 2004.
- [4] "The World Health Report - shaping the future," World Health Organization, 2003.
- [5] D. Abegunde, C. Mathers, T. Adam, M. Ortegón and K. Strong, "The burden and costs of chronic diseases in low-income and middle-income countries", *Lancet*, vol. 370, pp. 1929-1938, 2007.
- [6] WHO: World Health Report [www.who.int/whr/](http://www.who.int/whr/). 2007
- [7] Pfeffer MA, Braunwald E. Ventricular Remodeling After Myocardial-Infarction - Experimental-Observations and Clinical Implications. *Circulation* 1990;81:1161-1172.
- [8] Gheorghiade M, Bonow RO. Chronic heart failure in the United States - A manifestation of coronary artery disease. *Circulation* 1998;97:282-289.
- [9] Ulzheimer S, Flohr T: Multislice CT: Current Technology and Future Developments. In *Multislice CT*. Berlin, Heidelberg: Springer Berlin Heidelberg; 2009:3–23. [Medical Radiology].
- [10] Lin E, Alessio A: ScienceDirect.com - Journal of Cardiovascular Computed Tomography - What are the basic concepts of temporal, contrast, and spatial resolution in cardiac CT? *Journal of Cardiovascular Computed Tomography* 2009.
- [11] Buckley O, Rybicki FJ, Gerson DS, Huether C, Prior RF, Powers SL, Ersoy H. Imaging features of intramural hematoma of the aorta. *Int J Cardiovasc Imaging*. 2009.
- [12] Hsieh, J. *Computed tomography : principles, design, artifacts, and recent advances*. SPIE Optical Engineering Press; Bellingham, WA: 2003.
- [13] Flohr TG, McCollough CH, Bruder H, Petersilka M, Gruber K, Suss C, Grasruck M, Stierstorfer K, Krauss B, Raupach R, Primak AN, Kuttner A, Achenbach S, Becker C, Kopp A, Ohnesorge BM. First performance evaluation of a dual-source CT (DSCT) system. *Eur Radiol* 2006;16(2):256–268. [PubMed: 16341833].
- [14] McCollough CH, Schmidt B, Yu L, Primak A, Ulzheimer S, Bruder H, Flohr TG. Measurement of temporal resolution in dual source CT. *Med Phys* 2008;35(2):764–768. [PubMed: 18383698].

- [15] Araoz PA, Kirsch J, Primak AN, Braun NN, Saba O, Williamson EE, Harmsen WS, Mandrekar JN, McCollough CH. Optimal image reconstruction phase at low and high heart rates in dual-source CT coronary angiography. *Int J Cardiovasc Imaging*. 2009
- [16] Xu L, Yang L, Zhang Z, Li Y, Fan Z, Ma X, Lv B, Yu W. Low-dose adaptive sequential scan for dual-source CT coronary angiography in patients with high heart rate: Comparison with retrospective ECG gating. *Eur J Radiol*. 2009
- [17] Blankstein R, Shah A, Pale R, Abbara S, Bezerra H, Bolen M, Mamuya WS, Hoffmann U, Brady TJ, Cury RC. Radiation dose and image quality of prospective triggering with dual-source cardiac computed tomography. *Am J Cardiol* 2009;103(8):1168–1173. [PubMed: 19361609]
- [18] Blobel J, Baartman H, Rogalla P, Mews J, Lembcke A. [Spatial and temporal resolution with 16-slice computed tomography for cardiac imaging]. *Rofo* 2003;175(9):1264–1271. [PubMed: 12964084]
- [19] Herzog C, Arning-Erb M, Zangos S, Eichler K, Hammerstingl R, Dogan S, Ackermann H, Vogl TJ. Multi-detector row CT coronary angiography: influence of reconstruction technique and heart rate on image quality. *Radiology* 2006;238(1):75–86. [PubMed: 16373760]
- [20] Leschka S, Wildermuth S, Boehm T, Desbiolles L, Husmann L, Plass A, Koepfli P, Schepis T, Marincek B, Kaufmann PA, Alkadhi H. Noninvasive coronary angiography with 64-section CT
- [21] Coronary Computed Tomography Angiography Retrieved from <https://www.radiologyinfo.org/en/info.cfm?pg=angiocorocte>
- [22] Nieman, K., Cademartiri, F., Lemos, P. A., Raaijmakers, R., Pattynama, P. M. T., & de Feyter, P. J. (2002). Reliable Noninvasive Coronary Angiography With Fast Submillimeter Multislice Spiral Computed Tomography. *Circulation*, 106(16), 2051 LP-2054. Retrieved from <http://circ.ahajournals.org/content/106/16/2051>.
- [23] Russo, V., Gostoli, V., Lovato, L., Montalti, M., Marzocchi, A., Gavelli, G., ... Fattori, R. (2007). Clinical value of multidetector CT coronary angiography as a preoperative screening test before non-coronary cardiac surgery. *Heart*, 93(12), 1591–1598. <http://doi.org/10.1136/hrt.2006.105023>.
- [24] Manghat NE, Morgan-Hughes GJ, Broadley AJ, Undy MB, Wright D, Marshall AJ, Roobottom CA. 16-Detector row computed tomographic coronary angiography in patients undergoing evaluation for aortic valve replacement: comparison with catheter angiography. *Clin Radiol* 2006;61:749–57.
- [25] Leschka S, Alkadhi H, Plass A, Desbiolles L, Grünenfelder J, Marincek B, Wildermuth S. Accuracy of MSCT coronary angiography with 64-slice technology: first experience. *Eur Heart J* 2005;26:1482–7.

- [26] Ghostine S, Caussin C, Daoud B, Habis M, Perrier E, Pesenti-Rossi D, Sigal-Cinqualbre A, Angel CY, Lancelin B, Capderou A, Paul JF. Non-invasive detection of coronary artery disease in patients with left bundle branch block using 64-slice computed tomography. *J Am Coll Cardiol* 2006;48:1929–34.
- [27] Raff GL, Gallagher MJ, O'Neill WW, Goldstein JA. Diagnostic accuracy of noninvasive coronary angiography using 64-slice spiral computed tomography. *J Am Coll Cardiol* 2005;46:552–7.
- [28] Mollet NR, Cademartiri F, van Mieghem CA, Runza G, McFadden EP, Baks T, Serruys PW, Krestin GP, de Feyter PJ. High-resolution spiral computed tomography coronary angiography in patients referred for diagnostic conventional coronary angiography. *Circulation* 2005; 112:2318–23.
- [29] Leber AW, Knez A, von Ziegler F, Becker A, Nikolaou K, Paul S, Wintersperger B, Reiser M, Becker CR, Steinbeck G, Bookstegers P. Quantification of obstructive and nonobstructive coronary lesions by 64-slice computed tomography. *J Am Coll Cardiol* 2005;46:147–54.
- [30] Gilbert L. Raff, MD, FACC,\* James A. Goldstein, MD, FACC Coronary Angiography by Computed Tomography Coronary Imaging Evolves 2007; *J Am Coll Cardiol* 2007;49:1830–3.
- [31] D. B. Mark, D. S. Berman, M. J. Budoff, J. J. Carr, T. C. Gerber, H. S. Hecht, M. A. Hlatky, J. M. Hodgson, M. S. Lauer, J. M. Miller, R. L. Morin, D. Mukherjee, M. Poon, G. D. Rubin, and R. S. Schwartz, “ACCF/ACR/AHA/NASCI/SAIP/ SCAI/SCCT 2010 Expert Consensus Document on Coronary Computed Tomographic Angiography. A Report of the American College of Cardiology Foundation Task Force on Expert Consensus Documents,” *J. Am. Coll. Cardiol.* 55(23), 2663–2699 (2010).
- [32] ACR–NASCI–SPR Practice parameter for the performance and interpretation of cardiac Computed Tomography (CT), Resolution 39 (2014).
- [33] G. Shechter, J.R. Resar, and E.R. McVeigh, “Displacement and velocity of the coronary arteries: cardiac and respiratory motion,” *IEEE Trans. Med. Imaging* 25(3), 369–375 (2006).
- [34] L. Husmann, S. Leschka, L. Desbiolles, T. Schepis, O. Gaemperli, B. Seifert, P. Cattin, T. Frauenfelder, T. G. Flohr, B. Marincek, P. a Kaufmann, and H. Alkadhi, “Coronary artery motion and cardiac phases: dependency on heart rate -- implications for CT image reconstruction.,” *Radiology* 245(2), 567–576 (2007).
- [35] B. De Bruyne, W. F. Fearon, N. H. J. Pijls, E. Barbato, P. Tonino, Z. Piroth, N. Jagic, S. Mobius-Winckler, G. Rioufol, N. Witt, P. Kala, P. MacCarthy, T. Engström, K. Oldroyd, K. Mavromatis, G. Manoharan, P. Verlee, O. Frobert, N. Curzen, J. B. Johnson, A. Limacher, E. Nüesch, and P. Jüni, “Fractional flow reserve-guided PCI for stable coronary artery disease.,” *N. Engl. J. Med.* 371(13), 1208–17 (2014).
- [36] P. S. Douglas, G. Pontone, M. A. Hlatky, M. R. Patel, B. L. Norgaard, R. A. Byrne, N. Curzen, I. Purcell, M. Gutberlet, G. Rioufol, U. Hink, H. W. Schuchlenz, G. Feuchtner, M.

- Gilard, D. Andreini, J. M. Jensen, M. Hadamitzky, K. Chiswell, D. Cyr, A. Wilk, F. Wang, C. Rogers, and B. De Bruyne, "Clinical outcomes of fractional flow reserve by computed tomographic angiography-guided diagnostic strategies vs. usual care in patients with suspected coronary artery disease: the prospective longitudinal trial of FFRct: outcome and resource impacts stud," *Eur. Heart J.* ehv444 (2015).
- [37] P. Maurovich-Horvat, M. Ferencik, S. Voros, B. Merkely, and U. Hoffmann, "Comprehensive plaque assessment by coronary CT angiography," *Nat. Rev. Cardiol.* 11(7), 390–402 (2014).
- [38] Brodoefel H, Burgstahler C, Heuschmid M, Reimann A, Khosa F, Kopp A, Schroeder S, Claussen CD, Clouse ME. Accuracy of dual-source CT in the characterisation of non-calcified plaque: use of a colour-coded analysis compared with virtual histology intravascular ultrasound. *Br J Radiol.* 2009;82:805–812
- [39] Michelle C. Williams, MD, Amanda Hunter, MD, Anoop S.V. Shah, MD, Valentina Assi, PHD, Stephanie Lewis, PHD, Joel Smith, PHD, Colin Berry, MD, Nicholas A. Boon, MD, Elizabeth Clark, Marcus Flather, MD, John Forbes, PHD, Scott McLean, PHD, Giles Roditi, MD, Edwin J.R. van Beek, MD, Adam D. Timmis, MD, David E. Newby, MD, on behalf of the SCOT-HEART Investigators. Use of Coronary Computed Tomographic Angiography to Guide Management of Patients With Coronary Disease. *J. Am. Coll. Cardiol.* 67(15), 1759–1768 (2016).
- [40] Leber, A. W., Knez, A., Von Ziegler, F., Becker, A., Nikolaou, K., Paul, S., ... Boekstegers, P. (2005). Quantification of obstructive and nonobstructive coronary lesions by 64-slice computed tomography: A comparative study with quantitative coronary angiography and intravascular ultrasound. *Journal of the American College of Cardiology*, 46(1), 147–154. <https://doi.org/10.1016/j.jacc.2005.03.071>
- [41] Toepker, M., Euller, G., Unger, E., Weber, M., Kienzl, D., Herold, C. J., & Ringl, H. (2013). Stenosis quantification of coronary arteries in coronary vessel phantoms with second-generation dual-source CT: Influence of measurement parameters and limitations. *American Journal of Roentgenology*, 201(2), 227–234. <https://doi.org/10.2214/AJR.12.9453>
- [42] Kelm, B. M., Mittal, S., Zheng, Y., Tsymbal, A., Bernhardt, D., Vega-Higuera, F., ... Comaniciu, D. (2011). Detection, grading and classification of coronary stenoses in computed tomography angiography. *Lecture Notes in Computer Science (Including Subseries Lecture Notes in Artificial Intelligence and Lecture Notes in Bioinformatics)*, 6893 LNCS(PART 3), 25–32. [https://doi.org/10.1007/978-3-642-23626-6\\_4](https://doi.org/10.1007/978-3-642-23626-6_4)
- [43] Meyer, T., Hermann, F., Hadamitzky, M., Gerber, T. C., Mccollough, C., & Achenbach, S. (2009). Estimated Radiation Dose Associated With Cardiac CT Angiography, 301(5).
- [44] Lin, E. C. (2010). Radiation Risk From Medical Imaging. *Mayo Clinic Proceedings*, 85(12), 1142–1146. <https://doi.org/10.4065/mcp.2010.0260>

- [45] Tomizawa, N., Komatsu, S., Akahane, M., Torigoe, R., Kiryu, S., & Ohtomo, K. (2012). Relationship between beat to beat coronary artery motion and image quality in prospectively ECG-gated two heart beat 320-detector row coronary CT angiography. *The international journal of cardiovascular imaging*, 28(1), 139-146.
- [46] Contijoch, F., Stayman, J. W. and McVeigh, E. R. (2017), The impact of small motion on the visualization of coronary vessels and lesions in cardiac CT: A simulation study. *Med. Phys.*. doi:10.1002/mp.12295.
- [47] Bouma, H., Olivan Bescos, J., Villanova, A., & Gerritsen, F. A. (2007). Unbiased Vessel-Diameter Quantification based on the FWHM Criterion. *SPIE Medical Imaging*, 6512(July 2016). <https://doi.org/10.1117/12.709273>